9:
012136
1 OF 1

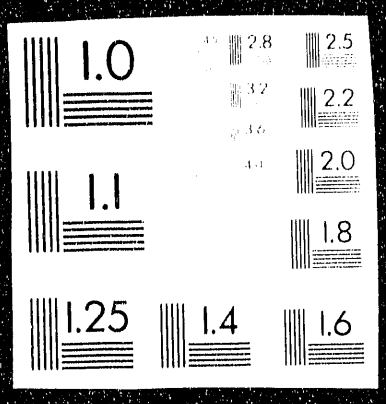

200nm

DOE/ER/45403--3

DE92 012136

ATOMIC STRUCTURES AND COMPOSITIONS OF INTERNAL INTERFACES

Progress Report
for Period September 1, 1991 to August 31, 1992

David N. Seidman

Northwestern University
Materials Science and Engineering Department
Evanston, Illinois 60208-3108

Karl L. Merkle

Argonne National Laboratory
Materials Science Division
Argonne, Illinois 60439-8269

March 1992

Prepared for

THE U. S. DEPARTMENT OF ENERGY
AGREEMENT NO. DE-FG02-89ER45403

MASTER

DISTRIBUTION OF THIS DOCUMENT IS UNLIMITED

DISCLAIMER

This report was prepared as an account of work sponsored by an agency of the United States Government. Neither the United States Government nor any agency thereof, nor any of their employees, makes any warranty, express or implied, or assumes any legal liability or responsibility for the accuracy, completeness, or usefulness of any information, apparatus, product, or process disclosed, or represents that its use would not infringe privately owned rights. Reference herein to any specific commercial product, process, or service by trade name, trademark, manufacturer, or otherwise does not necessarily constitute or imply its endorsement, recommendation, or favoring by the United States Government or any agency thereof. The views and opinions of authors expressed herein do not necessarily state or reflect those of the United States Government or any agency thereof.

ATOMIC STRUCTURES AND COMPOSITIONS OF INTERNAL INTERFACES

RESEARCH PROGRESS REPORT
FOR THE PERIOD 1 SEPTEMBER 1991 TO 31 AUGUST 1992

David N. Seidman, Principal Investigator
Materials Science and Engineering Department
Northwestern University
Evanston, Illinois 60208-3108
TEL: (708) 491-4391
FAX: (708) 491-7820

Karl L. Merkle, Co-Principal Investigator
Materials Science Divsion
Argonne, Illinois 60439-8269
(708) 972-4990

TABLE OF CONTENTS

ABSTRACT 2
INTRODUCTION 3
A. The Chemical Composition of a Metal/Ceramic Interface on an Atomic Scale: The Cu/MgO {111} Interface 3
1. Abstract 3
2. Introduction 3
3. Experimental Procedures 4
4. Transmission Electron Microscopy Results 5
5. High Resolution Electron Microscopy Results 6
6. Atom-Probe Field-Ion Microscope Results for Cu/MgO {111}-type Interfaces 7
7. Atom-Probe Field-Ion Microscope Evidence for Heterophase Fluctuations 16
8. Conclusions and Discussions 17
B. Chemical Composition on an Atomic Scale of Ni/Cr_2O_3 Interfaces 21
1. Abstract 21
2. Introduction 22
3. Experimental Procedures 22
4. Results 23
5. Conclusions 24

ABSTRACT

This research program addresses fundamental questions concerning the relationships between atomic structures and chemical compositions of metal/ceramic heterophase interfaces. The chemical composition profile across a Cu/MgO {111}-type heterophase interface, produced by the internal oxidation of a Cu(Mg) single phase alloy, is measured via atom-probe field-ion microscopy with a spatial resolution of 0.121 nm; this resolution is equal to the interplanar spacing of the {222} MgO planes. In particular, we demonstrate for the first time that the bonding across a Cu/MgO {111}-type heterophase interface, along a <111> direction common to both the Cu matrix and an MgO precipitate, has the sequence Cu|O|Mg... and *not* Cu|Mg|O... ; this result is achieved *without* any deconvolution of the experimental data. Before determining this chemical sequence it was established, via high resolution electron microscopy, that the morphology of an MgO precipitate in a Cu matrix is an octahedron faceted on {111} planes with a cube-on-cube relationship between a precipitate and the matrix. First results are also presented for the Ni/Cr_2O_4 interface; for this system selected area atom probe microscopy was used to analyze this interface; Cr_2O_4 precipitates are located in a field-ion microscope tip and a precipitate is brought into the tip region via a highly controlled electropolishing technique.

Introduction

This is a progress report on the experimental research program supported by the U. S. Department of Energy, Office of Basic Energy Sciences, under grant No. DE-FG02-89ER45403 that commenced 1 September 1989. The emphasis of this research program since it was initiated has been to obtain atomic scale information concerning the chemical sequencing across well-defined metal/ceramic interfaces. The metal/ceramic interfaces are produced by internally oxidizing binary metal alloys. The approach employed utilizes transmission electron microscopy, high resolution electron microscopy and atom probe field-ion microscopy. Transmission electron microscopy is employed to locate individual metal oxide precipitates in field-ion microscope specimens, high resolution electron microscopy is used to characterize the nature of the interface between a metal oxide precipitate and its matrix on an atomic scale, and atom probe field ion microscopy is used to determine the chemical nature of metal/ceramic interfaces. We have obtained result for two metal/metal oxide systems: Cu/MgO and Ni/Cr_2O_3. In the case of the Cu/MgO system, the atom probe is demonstrated to give unique and definitive chemical information with a depth resolution equal to 0.12 nm for the Cu/MgO system. The principal results for these two systems are detailed in Sections A and B below.

A. The Chemical Composition of a Metal/Ceramic Interface on an Atomic Scale: the Cu/MgO {111} Interface
(Dr. Ho Jang, Research Associate I)

1. Abstract

The chemical composition profile across a Cu/MgO {111}-type heterophase interface, produced by the internal oxidation of a Cu(Mg) single phase alloy, is measured via atom-probe field-ion microscopy with a spatial resolution of 0.121 nm; this resolution is equal to the interplanar spacing of the {222} MgO planes. In particular, we demonstrate for the first time that the bonding across a Cu/MgO {111}-type heterophase interface, along a <111> direction common to both the Cu matrix and an MgO precipitate, has the sequence Cu|O|Mg... and *not* Cu|Mg|O... ; this result is achieved *without* any deconvolution of the experimental data. Before determining this chemical sequence it was established, via high resolution electron microscopy, that the morphology of an MgO precipitate in a Cu matrix is an octahedron faceted on {111} planes with a cube-on-cube relationship between a precipitate and the matrix.

2. Introduction

Internal interfaces and, in particular, metal/ceramic heterophase interfaces are currently receiving a great deal of experimental attention because they are omnipresent in a wide range of materials and structures [1-6]; for example, metal matrix composites with ceramic fibers [7], metal/ceramic nanocomposites [8], machinable ceramics, metallization of microelectronic circuit structures [9], semiconductor devices, oxide scales on metals [10], and dispersion hardened alloys. The cohesive energies of metal/ceramic interfaces have also been the focus of much theoretical effort as ultimately the behavior of a metal/ceramic heterophase interface in service is determined by how well these rather disparate materials adhere to one another [11-14]. In particular, on the experimental side, a great deal of energy has been expended employing high resolution electron microscopy (HREM) to determine the terminating plane on the oxide side of metal/metal oxide heterophase interfaces by comparing HREM micrographs with micrographs computed using image simulation techniques [15-17].

In this paper we present the results of a different approach for studying the chemical character of metal/ceramic heterophase interfaces. We employ atom probe field-ion microscopy (APFIM) to directly ascertain -- on an atomic scale -- the chemical compositions of individual atomic planes in traversing Cu/MgO

I. Introduction and Research Highlights

This is a renewal proposal to continue the experimental research program supported by the U. S. Department of Energy, Office of Basic Energy Sciences, under grant No. DE-FG02-89ER45403 that commenced 1 September 1989. The emphasis of this research program since it was initiated has been to obtain atomic scale information concerning the chemical sequencing across well-defined metal/ceramic interfaces. The metal/ceramic interfaces are produced by internally oxidizing binary metal alloys. The approach employed utilizes transmission electron microscopy, high resolution electron microscopy and atom probe field-ion microscopy. Transmission electron microscopy is employed to locate individual metal oxide precipitates in field-ion microscope specimens, high resolution electron microscopy is used to characterize the nature of the interface between a metal oxide precipitate and its matrix on an atomic scale, and atom probe field ion microscopy is used to determine the chemical nature of metal/ceramic interfaces. We have obtained result for two metal/metal oxide systems: Cu/MgO and Ni/Cr_2O_3. In the case of the Cu/MgO system, the atom probe is demonstrated to give unique and definitive chemical information with a depth resolution equal to 0.12 nm for the Cu/MgO system. The principal results for these two systems are detailed in Sections A and B below.

A. The Chemical Composition of a Metal/Ceramic Interface on an Atomic Scale: the Cu/MgO {111} Interface
(Dr. Ho Jang, Research Associate I)

1. Abstract

The chemical composition profile across a Cu/MgO {111}-type heterophase interface, produced by the internal oxidation of a Cu(Mg) single phase alloy, is measured via atom-probe field-ion microscopy with a spatial resolution of 0.121 nm; this resolution is equal to the interplanar spacing of the {222} MgO planes. In particular, we demonstrate for the first time that the bonding across a Cu/MgO {111}-type heterophase interface, along a <111> direction common to both the Cu matrix and an MgO precipitate, has the sequence Cu|O|Mg... and *not* Cu|Mg|O... ; this result is achieved *without* any deconvolution of the experimental data. Before determining this chemical sequence it was established, via high resolution electron microscopy, that the morphology of an MgO precipitate in a Cu matrix is an octahedron faceted on {111} planes with a cube-on-cube relationship between a precipitate and the matrix.

2. Introduction

Internal interfaces and, in particular, metal/ceramic heterophase interfaces are currently receiving a great deal of experimental attention because they are omnipresent in a wide range of materials and structures [1-6]; for example, metal matrix composites with ceramic fibers [7], metal/ceramic nanocomposites [8], machinable ceramics, metallization of microelectronic circuit structures [9], semiconductor devices, oxide scales on metals [10], and dispersion hardened alloys. The cohesive energies of metal/ceramic interfaces have also been the focus of much theoretical effort as ultimately the behavior of a metal/ceramic heterophase interface in service is determined by how well these rather disparate materials adhere to one another [11-14]. In particular, on the experimental side, a great deal of energy has been expended employing high resolution electron microscopy (HREM) to determine the terminating plane on the oxide side of metal/metal oxide heterophase interfaces by comparing HREM micrographs with micrographs computed using image simulation techniques [15-17].

In this paper we present the results of a different approach for studying the chemical character of metal/ceramic heterophase interfaces. We employ atom probe field-ion microscopy (APFIM) to directly ascertain -- on an atomic scale -- the chemical compositions of individual atomic planes in traversing Cu/MgO

{111}-type interfaces that were produced by internal oxidizing [18-25] a Cu(Mg) single-phase alloy. This is a particularly interesting metal/ceramic interface as it involves the bonding of a noble free-electron metal (Cu) to a strongly heteropolar metal oxide (MgO). The heterophase interfaces formed by internal oxidation of Cu(Mg) have the following important advantages : (1) Impurity atom segregation is essentially nil -- atom probe observations substantiate this point -- because of the large total interfacial area per unit volume, (2) Common low index directions between the MgO precipitates and the matrix are present that have interplanar spacings suitable for HREM; and (3) All the MgO precipitates have a simple octahedral shape bounded by the low-index {111} planes. The APFIM technique is used to both supplement and complement transmission electron microscopy (TEM) and HREM observations of the same interface. Using APFIM we demonstrate in a direct manner -- *without* data deconvolution -- that the bonding across a Cu/MgO {111}-type interface, along a common <111> direction, has the bonding sequence Cu|O|Mg... and *not* Cu|Mg|O... ; the resolution for this chemical profiling is equal to the spacing between the {222} planes of MgO -- 0.121 nm.

3. Experimental procedures

Three different Cu(Mg) alloys were prepared by melting ASARCO copper (99.998+ at.% pure) and Johnson Matthey magnesium (99.98 at.% pure) in a high purity graphite crucible covered with a loose-fitting graphite cap; the copper was placed on top of the magnesium in the graphite crucible to confine the magnesium vapor during melting of the two elements. Prior to using the high purity graphite crucible it was heated for 4 hours at 1473 K under high vacuum conditions. The covered graphite crucible, containing the copper and magnesium charge, was placed in a quartz tube and evacuated to $1.3 \cdot 10^{-2}$ Pa, and then the quartz tube was backfilled with argon gas and sealed. The small cylindrically-shaped Cu(Mg) ingots produced in this manner each weighed approximately 26 gm. The particular alloy compositions prepared were Cu-0.16 at.% Mg, Cu-0.7 at.% Mg and Cu-2.8 at.% Mg; these Mg concentrations correspond to single-phase solid-solution alloys at 1173 K [26]. The ingots were rolled into 0.125 mm thick sheets for transmission electron microscopy (TEM) and HREM studies, or drawn into 250 μm diam wires for APFIM studies.

Cu/MgO internal interfaces were formed by internally oxidizing these alloy specimens utilizing the Rhines pack method [20,21]; this pack consists of a powder mixture of Cu plus Cu_2O plus Al_2O_3 (1:1:1), and it corresponds to heating the specimens in a partial pressure of oxygen equal to the decomposition pressure of cuprous oxide [21]. Figure 1 exhibits the root-mean squared-diffusion distance ($\sqrt{<X^2>}$) of the oxygen diffusion front versus time (t) for several internal oxidation temperatures and two different Mg concentrations -- 0.16 and 2.8 at.% Mg -- for a plate geometry. This plot was created from the experimental data presented in Ref. [21]. Fig. 1 demonstrates that the time required for complete internal oxidation decreases as the Mg concentration increases from 0.16 to 2.8 at.% Mg. This data also demonstrates that for the foil thickness we employ the value of $\sqrt{<X^2>}$ does not vary very much after ≈20 min, at several internal oxidation temperatures, for the 2.8 at.% Mg alloy. The time required to internally oxidize a cylinder completely is approximately 50% of the time to achieve the same condition for a plate [27]. Therefore, a 20 min treatment results in the complete internal oxidation of the 250 μm diam wires with 2.8 at.% Mg. To realize a high probability of finding an MgO precipitate in an APFIM specimen, experiments were performed to determine the optimum Mg concentration, internal oxidation temperature and time for achieving a high number density ($>5 \cdot 10^{21}$ m^{-3}) and small diam precipitates (<20 nm). The optimum composition for these combined experiments is a Cu-2.8 at.% Mg alloy, at an internal oxidation temperature of 1173 K, and an oxidizing time of 20 min for both the thin sheets and wires. These experiments demonstrate that to achieve the desired conditions the most critical parameter is the Mg concentration, and neither the temperature nor the time of the internal oxidizing treatment appear to be especially critical.

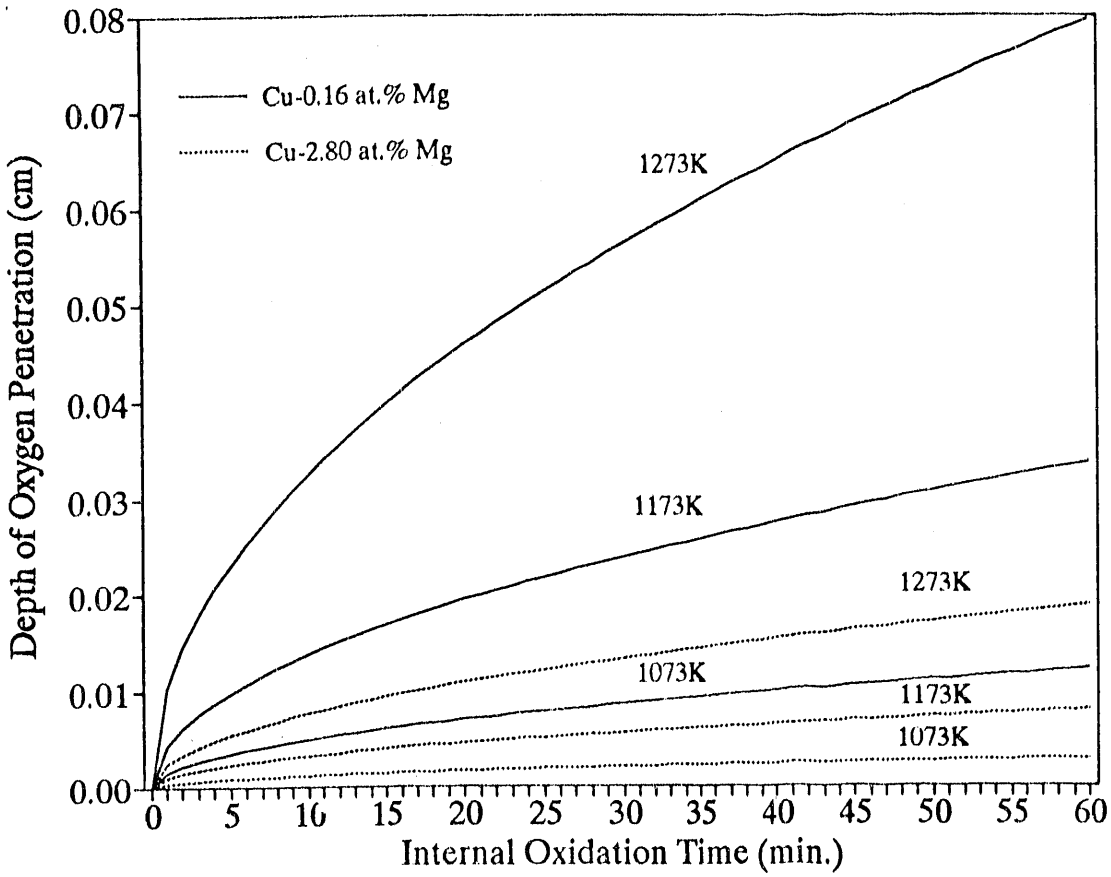

FIG 1. A plot of the root mean-squared diffusion distance ($\sqrt{\langle X^2 \rangle}$) for an oxygen diffusion front in Cu (Mg) alloys for two different Cu(Mg) alloys -- 0.16 and 2.8 at.% Mg. The curves were calculated employing data given in Ref. [21].

For the TEM and HREM studies 3 mm diam disks are punched out of the thin sheets, and a twin-jet polisher (Tenupol) employing a 30 vol.% nitric acid/70 vol.% methanol solution at 243 K is used to prepare electron transparent thin regions. The APFIM specimens are electropolished to a sharply-pointed tip with an approximately 25 nm diam, after the internal oxidation procedure, utilizing an electrolytic solution with the composition 100 g $Na_2CrO_4{:}4H_2O$ in 900 ml of acetic acid. A stainless steel cathode in the form of a 25 mm diam circular loop is used to electropolish the wire-shaped specimens and the electrolyte is placed in the loop to form a meniscus [28]. To examine the wire-shaped specimens by TEM a specially fabricated double-tilt stage is employed for an Hitachi 700H 200 kV electron microscope [28]. This double-tilt stage is unique as it allows us to examine the same wire FIM specimen both prior to and after an atom probe study, as well as at any stage of the electropolishing procedure [28].

4. Transmission electron microscopy results

First, conventional TEM is used to determine both the number density and size distribution of MgO precipitates in order to be certain that a precipitate is found in the small volume -- approximately 10^{-21} m^3 -- of an FIM tip, during the course of a pulsed-field evaporation dissection of a tip of an FIM specimen on an atom-by-atom basis. Figure 2(a) is a dark-field TEM micrograph -- recorded using a 020 operating reflection (g_{020}) -- of MgO precipitates in a Cu-2.8 at.% Mg alloy that had been internally oxidized employing the procedure

presented in Section 2. Note that these MgO precipitates in a Cu matrix exhibit typical "coffee-bean" strain-field contrast effects and that the line of no-contrast is perpendicular to g_{020} [29]. The contrast variations from precipitate to precipitate are due to the well-known depth oscillations with the position of a precipitate in a thin foil. Figure 2(b) is a bright field TEM micrograph taken along the [100] zone with many diffraction spots excited -- this is a so-called multibeam micrograph. From micrographs of the type shown in Fig. 2 we determine that the number density of MgO precipitates is approximately $5 \cdot 10^{21}$ m^{-3}; this density is high enough that MgO precipitates can be readily detected in the tip of an FIM specimen. (The histogram of the diameters of the MgO precipitates is quite broad [30]). The actual diameter of an MgO precipitate, however, is difficult to estimate precisely from the TEM micrographs exhibited in Fig. 2, since the observed shape and amount of strain-field contrast depend strongly on the direction of the electron beam relative to a specimen's crystallography [31,32].

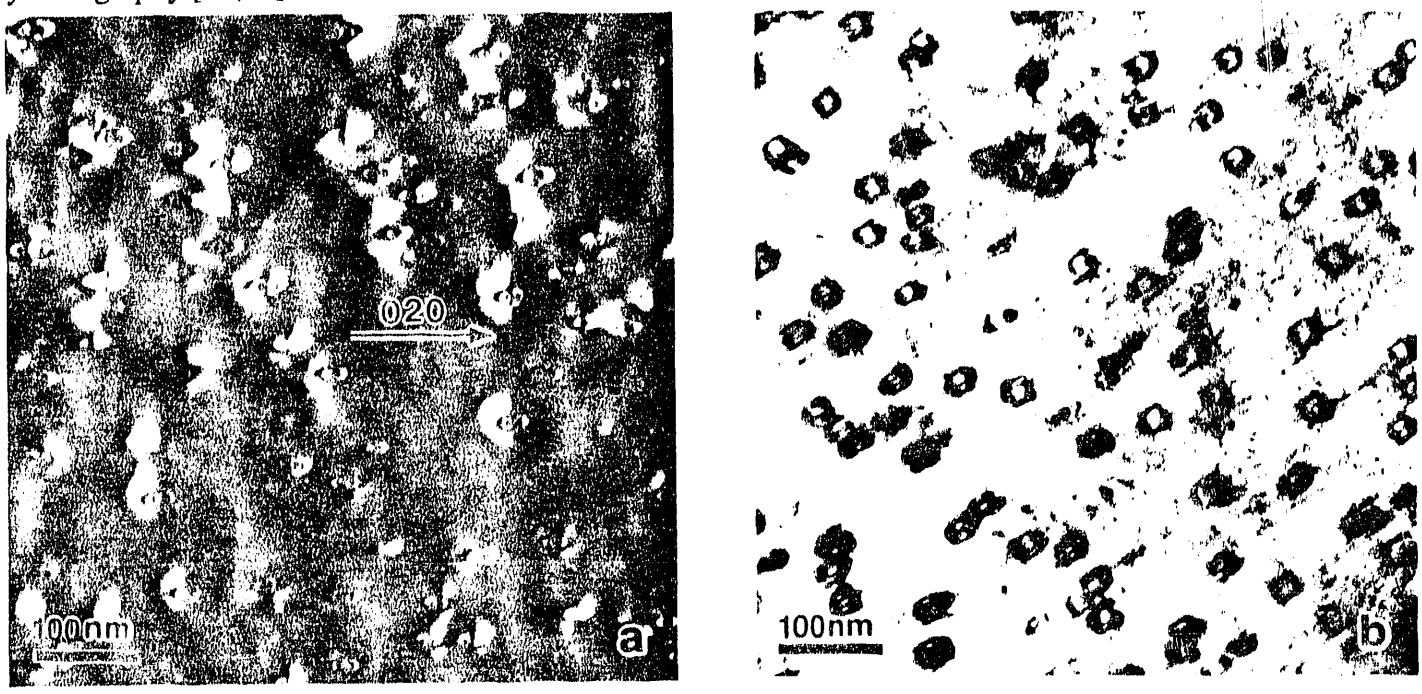

FIG. 2. (a) A dark-field transmission electron micrograph of MgO precipitates in a Cu matrix produced by internal oxidation of a Cu-2.8 at.% Mg alloy. The operating reflection is 020 (g_{020}) and the precipitates exhibit classical "coffee-bean" strain-field contrast . Note that the line of no-contrast is perpendicular to g_{020}. (b) A bright field transmission electron micrograph of MgO precipitates in a Cu matrix along a [100] zone axis with a number of reflections excited -- this is a so-called multibeam micrograph.

In view of the above, the Moiré fringe method is used to determine the exact dimensions of a precipitate -- it employs a double-diffraction technique [33]. For instance, Fig. 3 displays a TEM micrograph of MgO precipitates that exhibit parallel $(11\bar{1})$ Moiré fringes of a faceted precipitate -- the operating reflection for this micrograph is $11\bar{1}$ ($g_{11\bar{1}}$) -- with the projected image plane close to (123). And, therefore, the shape of the fringes represents the shape of the precipitate viewed along a [123] direction. The Moiré pattern in this case is a result of the difference between the interplanar spacings of the Cu and MgO $(11\bar{1})$ lattice planes. The fringe spacing is 1.5 nm and the average diameter of the precipitates studied by this technique is 19.5 nm.

5. High Resolution Electron Microscopy Results

To investigate the detailed atomic structure of a Cu/MgO {111}-type heterophase interface and to learn more about its geometric shape,HREM observations were performed on Cu-2.8 at.% Mg specimens that had

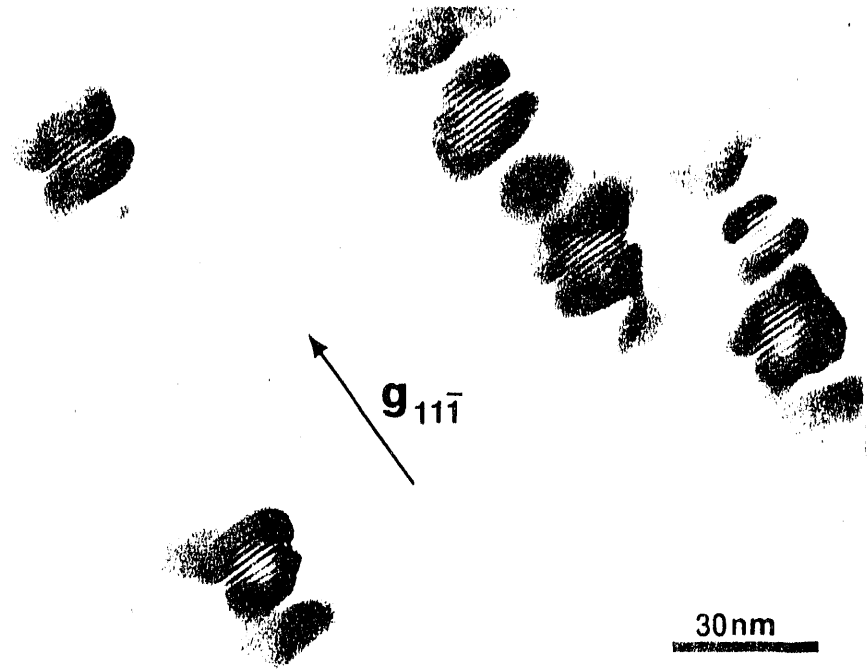

FIG. 3. A (111) Moiré fringe pattern of a faceted MgO precipitate with the image plane close to (123). The shape of the fringes represents the shape of the precipitate viewed along a [123] direction. The strain-field contrast pattern near the MgO precipitates displays a different shape compared to the pattern seen in Fig. 2; this illustrates that the contrast changes according to the orientation of the specimen relative to the electron beam.

been internally oxidized as described in Section 2. Axial illumination in an Hitachi H9000 HREM allows the direct observation of the configuration of atoms near an internal interface when proper operating conditions are met [34]. The high resolution micrographs now discussed demonstrate that the MgO precipitates have an octahedral shape. First, Fig. 4 exhibits an HREM image (defocus value is 69.4 nm at 300 kV) of an MgO precipitate in a Cu matrix with a common [100] zone axis for both the MgO precipitate and the Cu matrix. The 0.21 nm interplanar spacing of the (200) planes of this MgO precipitate is indicated on it, and the 0.181 nm interplanar spacing of the (020) planes of the copper matrix is also indicated. Note that the projection of this precipitate on the (100) plane is an approximately square-shaped figure; two of the sides are, however, slightly curved -- this is because this precipitate is not fully relaxed to its equilibrium shape [34,35]. The truncation of an octahedron by the {100}-type planes gives rise to squares of different dimensions. Second, Fig. 5 is a HREM image (defocus value of 65.1 nm at 300 kV) recorded employing a common [110] zone axis for an MgO precipitate in a Cu matrix. This micrograph shows quite clearly that the projection of this precipitate on a (110) plane has an hexagonal-shape, although it is not a perfect hexagon because the precipitate is not fully relaxed; the hexagonal shape arises from the truncation of an octahedron by {110}-type planes, when they do not pass through its apex. The 0.242 nm interplanar spacing of the $(\bar{1}11)$ planes of this MgO precipitate is indicated on it, and the 0.209 nm interplanar spacing of the $(1\bar{1}1)$ planes of the copper matrix is also indicated. The diam of this MgO precipitate is 13 nm. Third, Fig. 6 is a HREM (defocus value of 65.1 nm) also recorded employing a common [110] zone axis exhibiting a diamond-shaped MgO projection on the (110) plane; this shape is a result of the truncation of an octahedron by a {110}-type plane passing through its apex. These HREM images also demonstrate that the orientation relationship is cube-on-cube with the Cu matrix, as found in previous investigations [17,34,35], with an octahedral-shaped precipitate that is faceted on {111} planes. The lattice misfit parameter (η) is given by $\eta = 2[(a_{MgO} - a_{Cu})/(a_{MgO} + a_{Cu})]$, where the a's are the lattice parameters of the two phases, and its experimental value is 0.1483 in agreement with the calculated value; $a_{Cu} = 0.362$ nm and

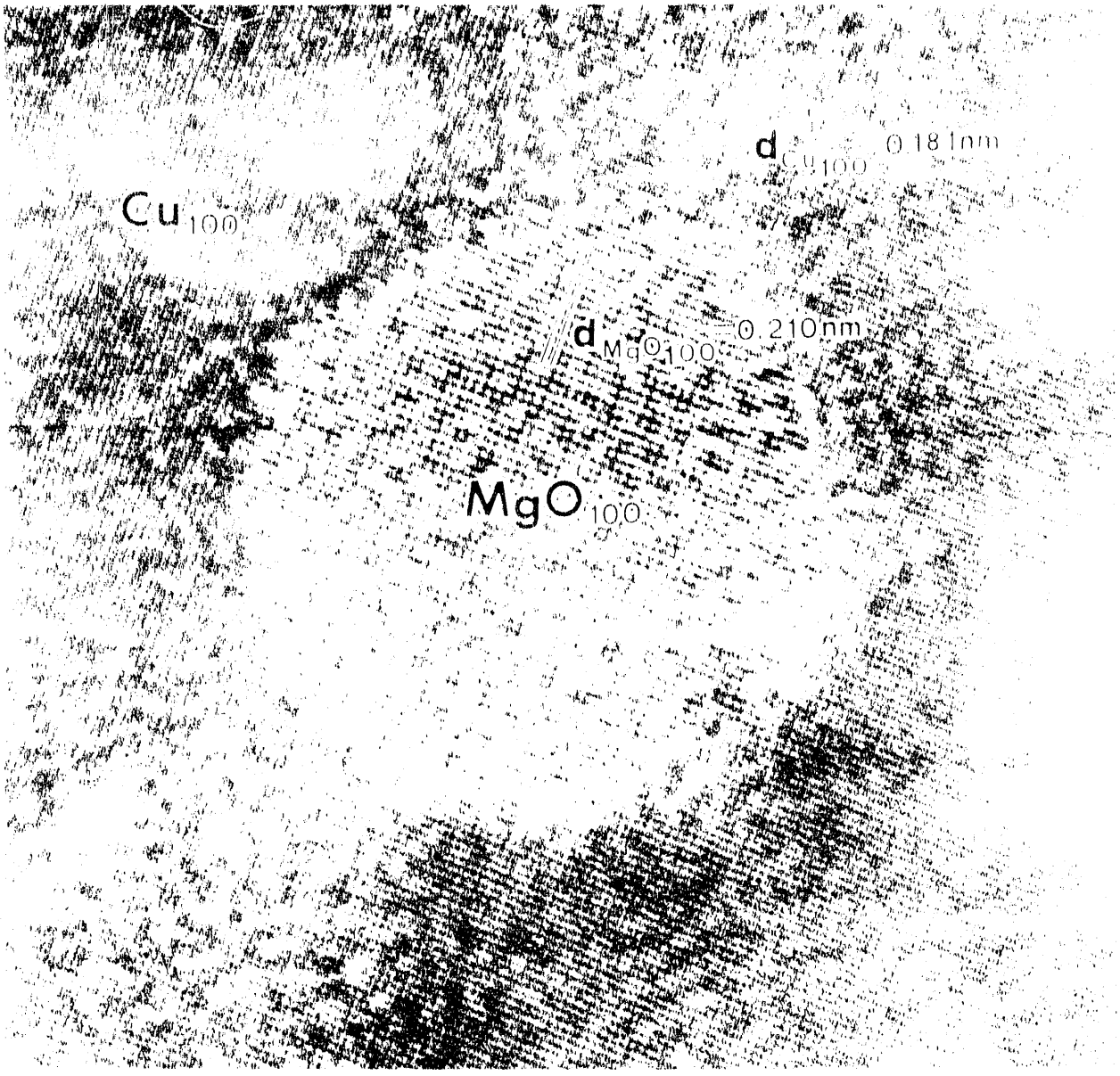

FIG. 4. [illegible] electron microscope image of an MgO precipitate in the Cu matrix [illegible] defocus value is 69.4 nm at an operating voltage of 300 kV. [illegible] in the MgO precipitate is indicated on the precipitate [illegible] in the Cu matrix is indicated on it. The atomic [illegible] some crystallographic orientationship relationship [illegible]

[illegible] HRTM micrograph recorded employing a common [illegible] misfits dislocations at the interface between an MgO [illegible] approximately [illegible]

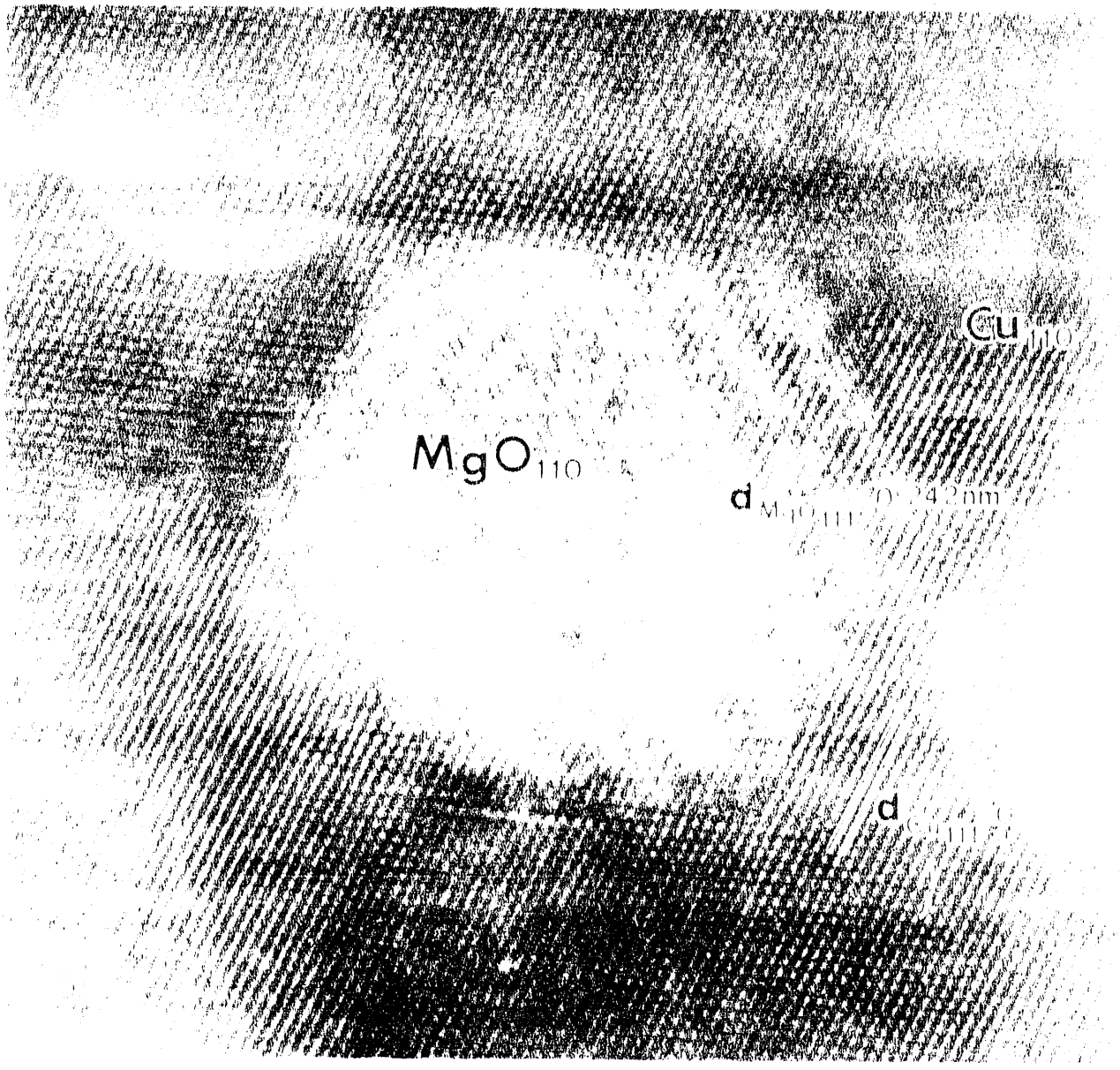
Cu
MgO110
d

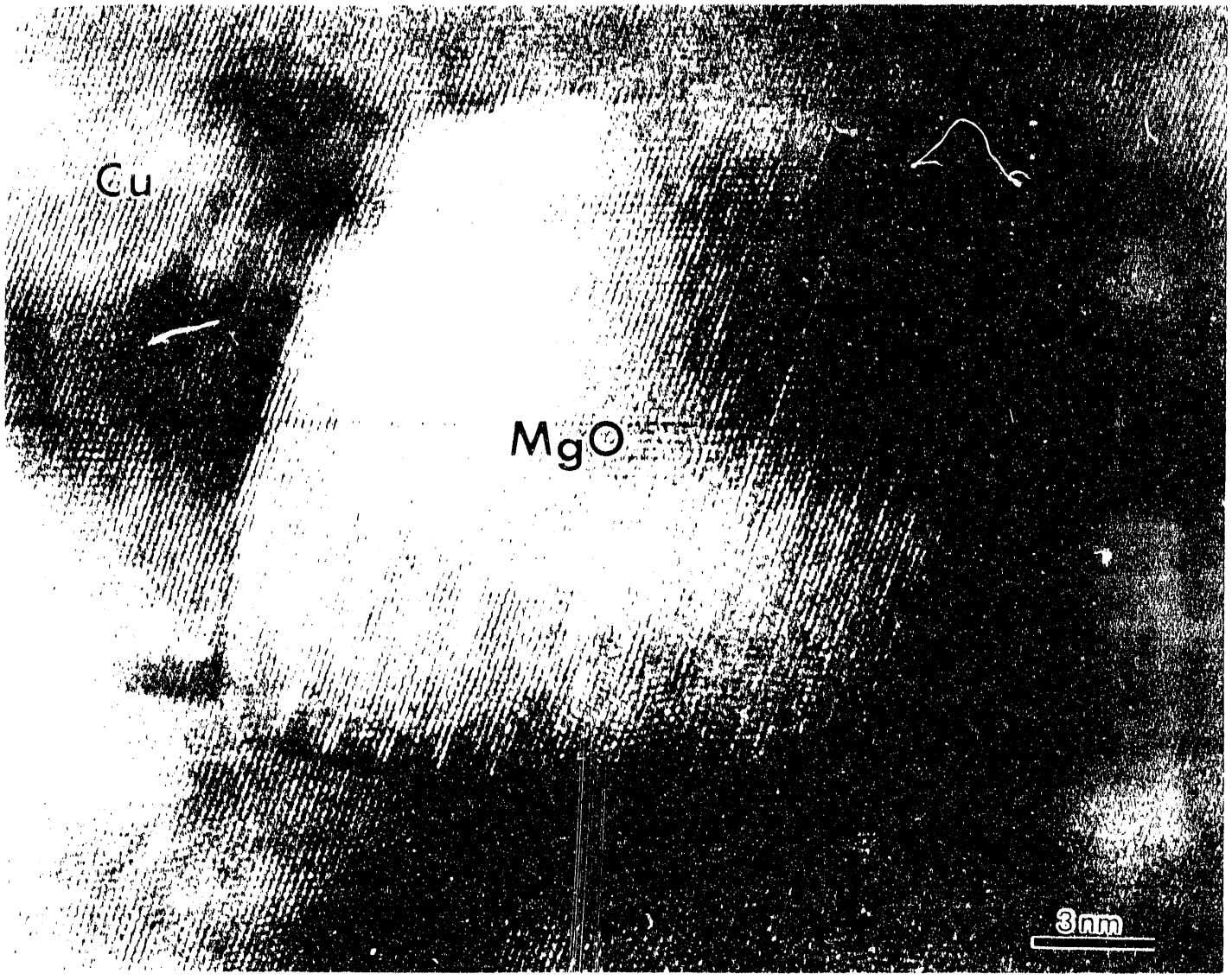

FIG. 6. A high resolution electron microscope of an MgO precipitate in the Cu matrix viewed along a common [110] zone axis; defocus value is 65.1 nm and the operating voltage is 300 kV. The truncation of an MgO precipitate by (110) planes results in a diamond-shaped image, as is expected when (110) planes pass through the apex of an octahedron.

6. Atom-probe field-ion microscope results for Cu/MgO {111}-type interfaces

For a chemical analysis of a Cu/MgO {111}-type interface a sharply pointed atom-probe specimen with a tip radius of approximately 65.8 nm, in the region of the (111) pole, is employed. Figure 9 is a TEM micrograph of an FIM specimen containing MgO precipitates. From this TEM micrograph it is seen that the FIM specimen contains uniformly aligned MgO precipitates exhibiting a directional consistency with respect to the fiber axis of the wire. This axis is a [111] direction as determined from careful TEM tilting experiments. Hence this observation is consistent with the known experimental results on wire textures of [illegible] [illegible] noted, however, that recrystallized Cu can exhibit several different textures [illegible] [100], [illegible] depending on the amount of plastic reduction, the alloying element and annealing temperature [illegible] the number density of MgO precipitates is high enough that the pulsed field evaporation [illegible] specimen on an atom by atom basis is likely to result in the intersection of the surface of the FIM [illegible]

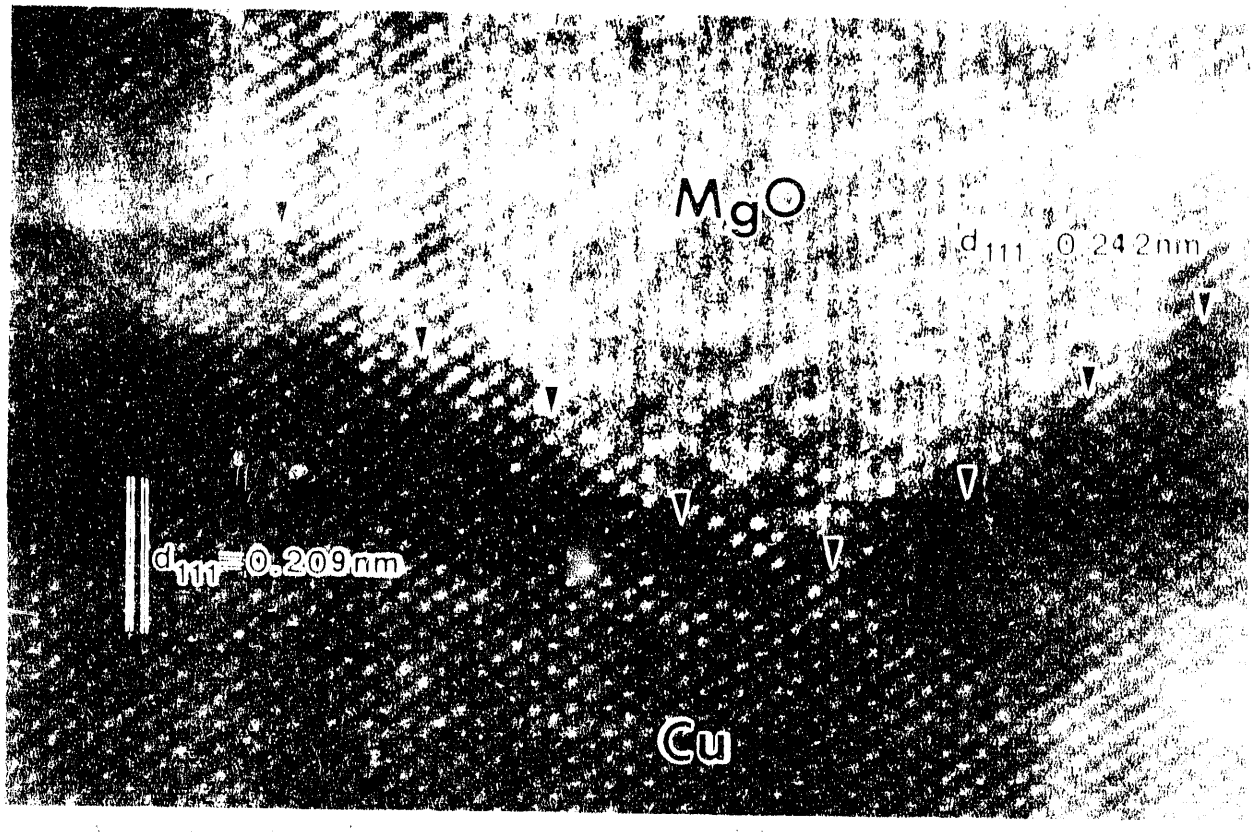

FIG. 7

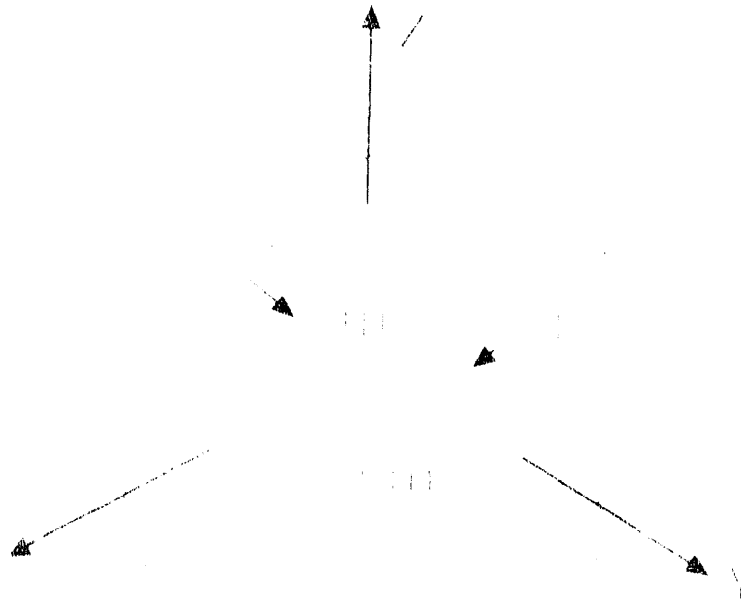

FIG. 8

FIG. 9. A transmission electron micrograph of a field-ion microscope specimen containing a high number density of MgO precipitates. The MgO precipitates are all aligned in the same direction with respect to the matrix -- that is, along a <111>-type direction; thus, a {111}-type plane of the MgO precipitates is parallel to a corresponding {111}-type plane of the Cu matrix.

precipitate on a random basis. This is a crucial point, for if the number density of precipitates is not high enough then the probability of finding a precipitate in the volume of an FIM tip is essentially nil. Alternatively it is possible to use a combination of TEM and careful electrochemical backpolishing techniques to place a preselected metal oxide precipitate in the field-of-view of a field-ion microscope image [28,37].

Figure 10 is a schematic drawing illustrating the relationship between an MgO precipitate and the chevron ion detector in the atom probe. The MgO precipitate sits in an FIM specimen such that a {111}-type plane is parallel to the channel electron multiplier array containing a circular probe hole; that is, for instance, a (111) bounding plane of an octahedral-shaped MgO precipitate is parallel to a (111) plane of the Cu matrix. The distance from the probe hole to the FIM is typically between 4 to 6 cm, and the distance from the FIM tip to the chevron detector is approximately 2.2 m; the chevron detector consists of two channel electron multiplier arrays in series to yield a gain of $\approx 10^6$ for a single ion [38]. The projected diameter of the probe hole on the surface of the FIM tip is varied by changing the distance between the FIM specimen and the channel electron multiplier array [38]. In the cases to be discussed -- see Figs. 13 to 15 -- this distance was adjusted such that the projected diameter of the probe hole is less than the diameter of a precipitate. A pulsed dissection process consists of applying a series of pulse voltages (V_p) on top of a steady-state imaging voltage (V_{dc}) as this results in the dissection of a specimen on an atom-by-atom basis; pulsed field-evaporation is a highly controllable process that has been successfully employed to observe individual point defects -- vacancies and self-interstitial atoms -- in the bulk of specimens [39] as well as small precipitates in metal alloys [40-44]. As illustrated in Fig. 10 all the atoms in the cylinder of material with the diameter D are analyzed -- that is, their mass-to-charge state ratios are determined -- on an atom-by-atom basis. For the geometry illustrated in Fig. 10 *no* matrix correction to the composition of a precipitate is required; alternatively, if the diameter of a precipitate is greater than the projected diameter of the probe hole on a precipitate then there is a *potential* correction to a precipitate's composition. In the case of MgO precipitates there is no solid solubility of Cu in MgO; hence, even if Cu is detected while dissecting a precipitate this is Cu from the matrix and not from the precipitate; the problem of the matrix contribution to a precipitate has been dealt with in some detail elsewhere [45].

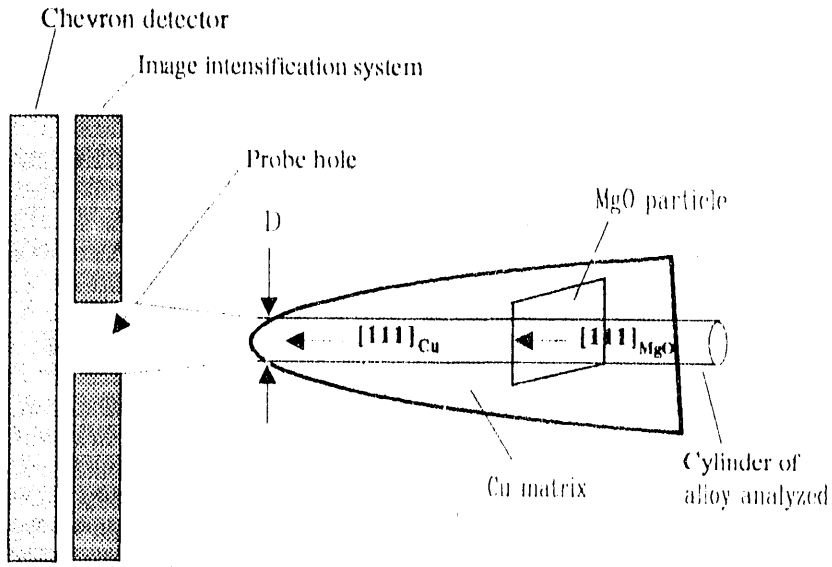

FIG.10. The geometry employed for analyzing a Cu/MgO interface, with the plane of the channel electron multiplier array containing the probe hole parallel plane to a {111} plane of the MgO precipitate. The projected diameter of the probe hole on the surface of the field ion microscope tip is indicated by the letter D. The pulsed field-evaporated ions pass through the probe hole in the channel electron multiplier array on their journey to the chevron detector; the latter consists of two channel electron multiplier arrays in series with an overall gain of 10^6 for an individual ion. The distance from the field ion microscope tip to the channel multiplier array is typically between 4 to 6 cm, while the distance to the the chevron detector is ≈2.2 m. The spatial resolution of a composition profile across the Cu/MgO {111} interface -- along a common <111> direction -- is determined by the interplanar spacing of the {111} planes of an MgO precipitate -- 0.121 nm. This schematic diagram is *not* to scale.

The same specimen exhibited in Fig. 9 was then transferred to our atom probe for a chemical analysis of a {111}-type interface. Figure 11 is an FIM micrograph exhibiting an MgO precipitate in the Cu matrix of this specimen. Note well that the heterophase interface of the MgO precipitate is parallel to the (111) planes of the Cu matrix; this is consistent with the HREM observations, and it also implies that the exposed plane of the precipitate is a $(111)_{MgO}$ plane. The approximate diam of this precipitate is 7.3 nm. Note the projection of the probe hole in the channel electron multiplier array onto the FIM image at approximately 3 o'clock near the 111 pole. Figure 12 is a series of FIM micrographs recorded at various stages of a pulsed field-evaporation dissection sequence of this MgO precipitate; the actual dissection process is on an atom-by-atom basis, and these six FIM images are simply representative of this process. Image 1 is at the beginning of the pulsed-field dissection process of this precipitate, and by image 6 the MgO precipitate has been completely removed by it; the black arrow heads point at the MgO precipitate. It is emphasized that both the MgO precipitate and the Cu matrix are simultaneously removed by this dissection technique -- see Figure 10. Also note that individual atoms within the MgO precipitate are resolved at different stages of its dissection; furthermore, the precipitate exhibits well-developed contrast features outlining its atomic scale geometry.

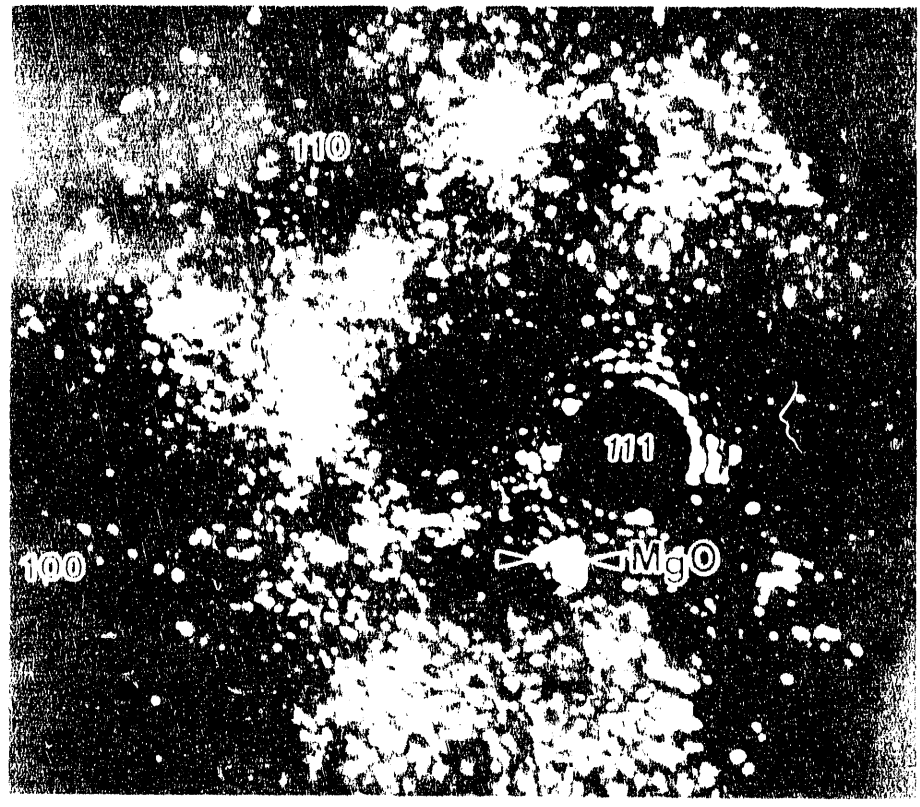

Fig. 11. [illegible]

[illegible] is a histogram of the number of events versus the [illegible] MgO precipitate, the ordinate is a logarithmic scale while [illegible] dominated by the Cu peaks due to the presence of [illegible] the two peaks for each charge state are due to the two naturally occurring [illegible] Also note the presence of singly and doubly charged O [illegible] as well as singly charged Mg ions from an MgO [illegible] charged H ions is also present, this peak is from the [illegible] was performed at a background pressure of [illegible]

For [illegible] containing MgO precipitates the pulse fraction [illegible] and a pulse frequency of 15 Hz is used to [illegible] evaporation technique [39]. The detection efficiency [illegible] field evaporation pulses is maintained at [illegible] the value of V_{dc} is automatically increased [illegible]

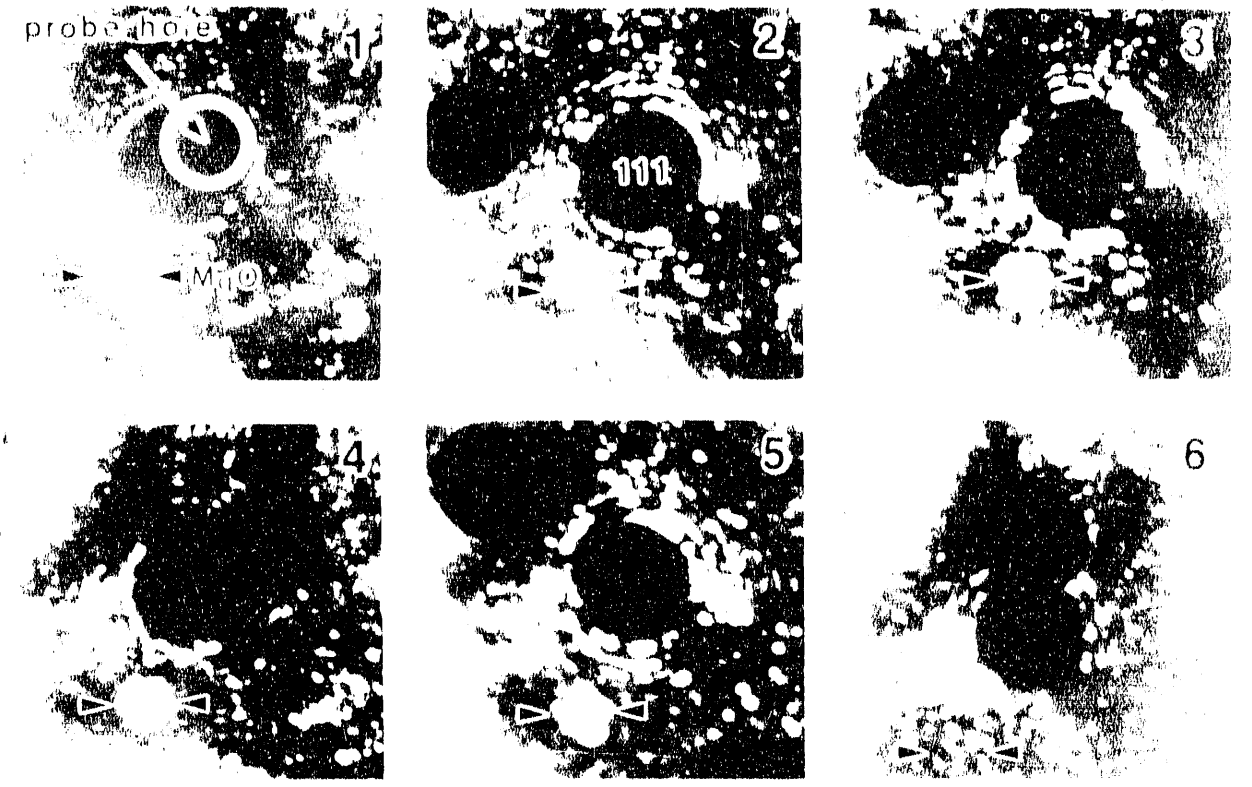

FIG. 12. [illegible] of FIM images showing the pulse dissection of [illegible] MgO [illegible] Cu matrix, the (111) plane of the MgO [illegible] matrix. Note that individual atoms within a (222) plane of the MgO [illegible] [illegible] temperature is 40 K.

[illegible] specimen was placed at a [illegible] approximately 70 atoms [46, 48].

Figure 13 [illegible] an integral profile of the cumulative number of Mg or O ions versus the [illegible] of Cu plus Mg plus O ions [49]. It was created by performing a random area analysis along a [illegible] the Cu matrix. The Cu signal on the ordinate is omitted for clarity because of the large differ[illegible] value and the Mg or O [illegible].

The projected diameter of the probe hole on the tip is smaller than the diameter of the MgO [illegible] no correction to the data is required because of a possible matrix [illegible] precipitate [illegible] [48]. It is seen from this integral profile that the matrix is essentially [illegible] the Cu/MgO [illegible] interface, prior to the Cu/MgO (111) interface only 13 oxygen events were [illegible] total of 10 [illegible] O plus Mg events for a bulk concentration of [illegible] at. fr. oxygen, in addition [illegible] Mg event was [illegible] for a bulk concentration of [illegible] at. fr. magnesium. Note carefully [illegible] outermost (222) plane of ions of the MgO precipitate consists *solely* of oxygen ions, and the second [illegible] [illegible] ions. (At this point the specimen failed catastrophically, presumably [illegible] ion is considerably lower than that of an oxygen ion.) The [illegible] interplanar [illegible] along the (111) direction in the MgO [illegible] [illegible] from the Cu matrix [illegible] the MgO [illegible] precipitate [illegible] (111) interface [illegible]

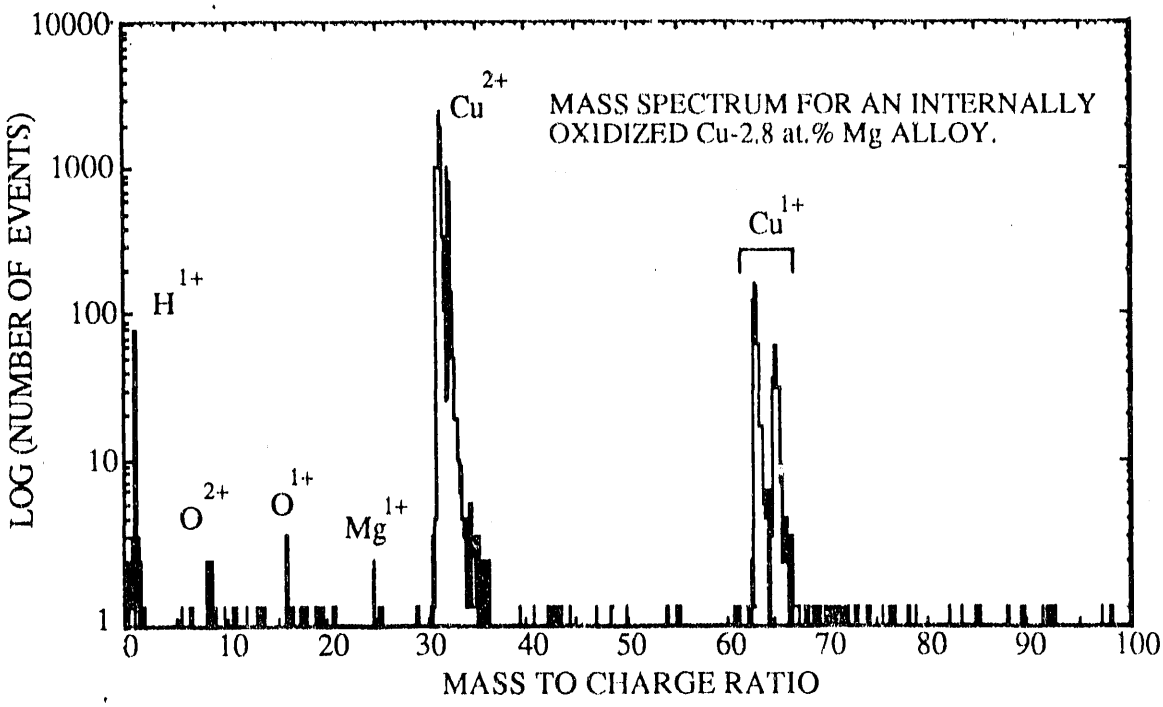

FIG. 13. An atom-probe field-ion microscope mass spectrum of an internally oxidized Cu/MgO specimen. The ordinate is the number of events plotted on a logarithmic scale, while the abscissa is the mass-to-charge state ratio of the pulsed field-evaporated ions. This spectrum was recorded at a background pressure of $1.2 \cdot 10^{-8}$ Pa employing a pulse fraction (f) of 0.1; f is the ratio of the pulsed field evaporation voltage (V_p) to the steady-state voltage (V_{dc}) on a field-ion microscope specimen. The hydrogen ion signal is from the background pressure in the atom probe.

Figure 15 is an integral profile along a [111] direction across a Cu/MgO (111) interface in another octahedral-shaped MgO precipitate. In this case no Mg events were detected in the matrix while 7 oxygen events were detected out of a total of 815 events, and this implies of a bulk concentration of $<10^{-3}$ at. fr. magnesium and $8.6 \cdot 10^{-3}$ oxygen. Once again, there is an abrupt transition from an essentially pure Cu matrix to a (222) plane in the precipitate that is 100 at.% oxygen, and then the second (222) plane is 100 at.% magnesium (again the tip then failed catastrophically). The depth resolution is 0.121 nm for this profile just as it is in Fig. Fig. 14. Thus once again the experimental results for this precipitate demonstrate directly -- that is, *without* data deconvolution -- that the bonding across a Cu/MgO (111) interface has the sequence Cu|O|Mg|... and *not* Cu|Mg|O|... .

7. Atom Probe Field-Ion Microscope Evidence for Heterophase Fluctuations

Figure 16 is an integral profile for oxygen or magnesium along a <110>-type direction; this is a long run that consists of a total of 30,000 copper plus magnesium plus oxygen ions; the Cu integral profile is not exhibited because of the problem of simultaneously displaying the number of Cu, Mg and O ions on the same ordinate scale . Note the three highly localized changes in the oxygen and magnesium concentrations denoted by the numbers 1, 2 and 3. These regions correspond to small heterophase fluctuations or clusters of magnesium oxide -- that is, the final stoichiometric ratio of one Mg atom to one O atom has not yet been achieved. Note that for each cluster the concentration of magnesium is greater than the oxygen concentration. This is significant as it indicates that the results cannot be explained on the basis of preferential field evaporation; if this is the case then the Mg should be preferentially field evaporated as it has a significantly lower cohesive energy than does oxygen; the cohesive energies of Mg and O are 1.51 eV $atom^{-1}$ and 2.60 eV $atom^{-1}$ respectively [50], and the evaporation field is to first order determined by the cohesive energy [51,52].

The ability of the atom probe to detect heterophase fluctuations [53] was discovered during the course of examining a specimen that had a mean MgO precipitate diamter of less than 10 nm.

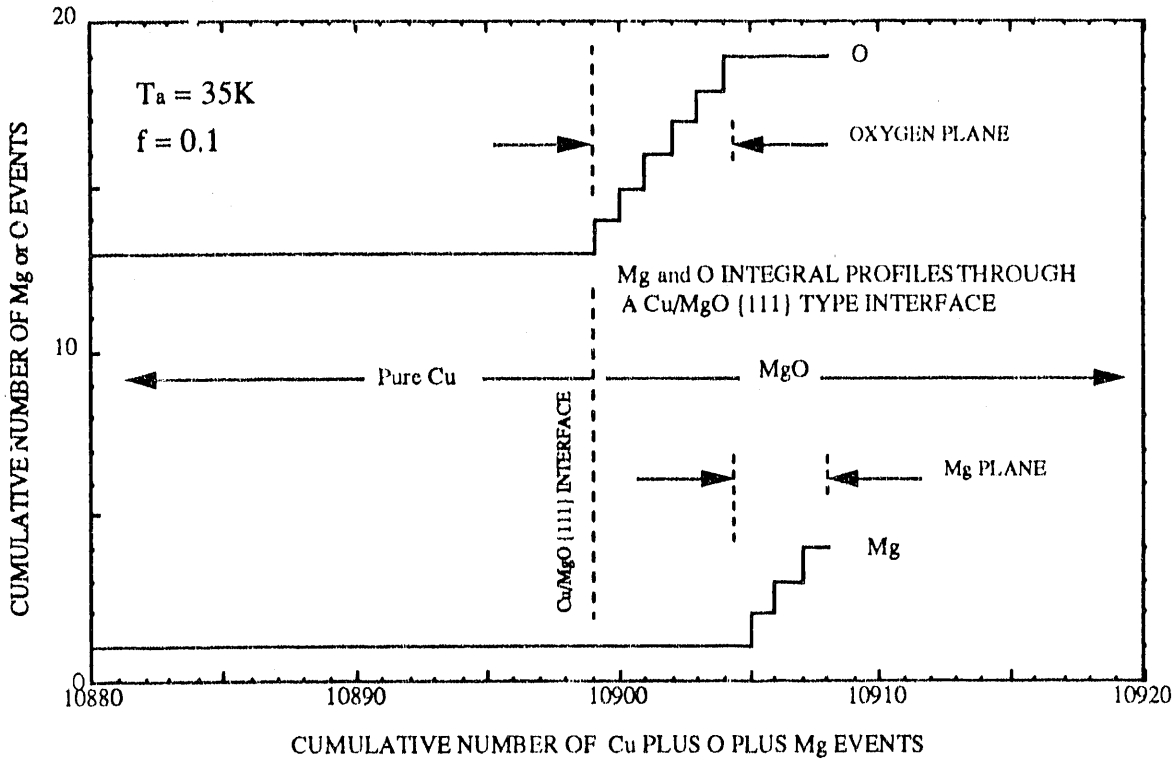

FIG.14. Integral profiles across a Cu/MgO (111) interface detected during a random area analysis along a [111] direction. The cumulative number of Mg or O ions detected is plotted versus the cumulative number of Cu plus Mg plus O ions detected. The data were collected for a specimen temperature of 35 K, a pulse fraction of 0.1, a pulse frequency of 15 Hz, and a background pressure of $1.2 \cdot 10^{-8}$ Pa. The Cu signal -- not exhibited -- disappears at the Cu/MgO (111) interface and then the signal is 100 at. % oxygen until that (222) plane has been completely removed by the field-evaporation process, and then the next (222) plane is found to be 100 at. % magnesium. This result indicates directly that the sequence of (111) planes across this heterophase interface is Cu|O|Mg... . The depth resolution for this chemical composition profile is $a_0/(2\sqrt{3})$, where a_0 is the lattice parameter of MgO (0.420 nm), and is equal to 0.121 nm. The data displayed in this integral profile have *not* undergone any deconvolution process. Note that the number of oxygen events detected before the Cu/MgO interface is reached is 13 out of a total number of 10,899 events (Cu plus Mg plus O); and the number of Mg events detected before this same interface is reached is 1 out of a total of 10,899 events (Cu plus Mg plus O); thus the respective concentrations in the Cu matrix are $\approx 10^{-3}$ at. fr. oxygen and $9 \cdot 10^{-5}$ at. fr. magnesium.

8. Conclusions and Discussions

1. Three different Cu(Mg) alloys -- 0.16, 0.7 and 2. 8 at. % Mg -- were internally oxidized in order to find an alloy composition, annealing temperature and time that yields a high number density ($5 \cdot 10^{21}$ m^{-3}) of small (<20 nm diam) MgO precipitates.

2. A transmission electron microscope study of internally oxidized field-ion microscope specimens of these alloys demonstrated that the number density and diameters achieved -- see preceding point -- for the 2.8 at.% Mg alloy are suitable for performing atom probe field-ion microscope studies of those specimens to determine the Cu/MgO interfacial chemistry on an atomic scale. The optimum internal oxidation conditions for

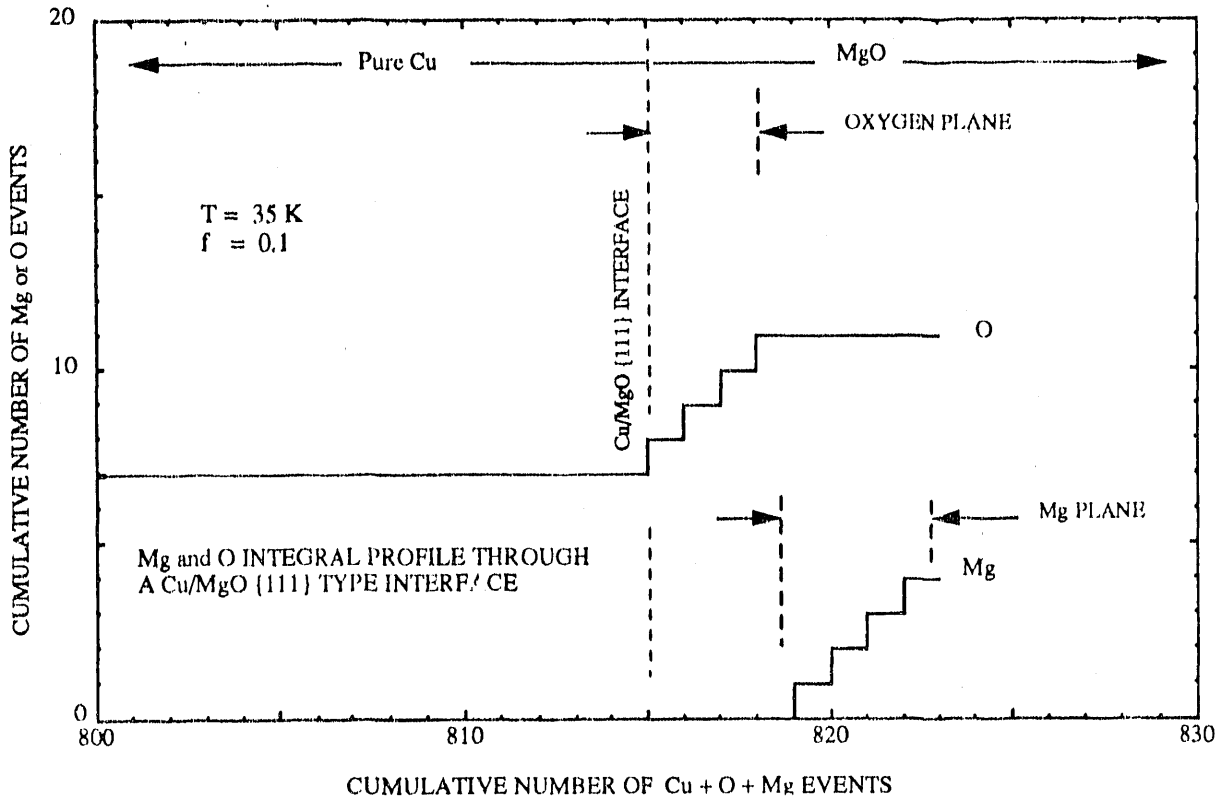

FIG. 15. Another integral profile across a Cu/MgO (111) interface detected during a random area analysis along a [111] direction. The cumulative number of Mg or O ions detected is plotted versus the cumulative number of Cu plus Mg plus O ions detected. The data were collected for a specimen temperature of 35 K, a pulse fraction of 0.1, a pulse frequency of 15 Hz, and a background pressure of $1.2 \cdot 10^{-8}$ Pa. The Cu signal -- not exhibited -- disappears at the Cu/MgO interface and then the signal is 100 % oxygen until that plane has been completely removed by the field evaporation process, and then the next (111) plane is 100 % magnesium. This result indicates directly that the sequence of planes across this heterophase interface is Cu|O|Mg... . Note that the number of oxygen events detected before the Cu/MgO interface is reached is 7 out of a total number of 815 (Cu plus Mg plus O); and the number of Mg events detected before this same interface is reached is zero out of a total of 815 events (Cu plus Mg plus O); thus the respective concentrations in the Cu matrix are $<8.6 \cdot 10^{-3}$ at. fr. oxygen and $<\approx 10^{-3}$ at. fr. magnesium.

our experiments are a time of 20 min at 1173 K for this alloy. The most critical parameter appears to be the Mg concentration.

3. A high resolution transmission electron microscope study of MgO precipitates in a Cu matrix along the [100] or [110] axial directions demonstrates that the precipitates have the morphology of an octahedron with the facets corresponding to {111} planes. The orientationship relationship between the MgO precipitate and the Cu matrix is cube-on-cube.

4. The MgO precipitates are semi-coherent with the Cu matrix even though the lattice misfit parameter (η) is 0.1483; η is given by $2[(a_{MgO} - a_{Cu})/(a_{MgO} + a_{Cu})]$ where the a's are the lattice parameters of the two phases. Misfit dislocations are detected at the Cu/MgO {111}-type heterophase interface, suggesting that the 0.1483 misfit between the MgO precipitate and the Cu matrix is accommodated by a combination of dislocations and elastic straining.

5. The MgO precipitates are readily detectable by field-ion microscopy. A recrystallization texture of the Cu wires is fortuitously [111], hence the MgO precipitates sit in the Cu matrix such that the (111) facets of the octahedral-shaped precipitates are perpendicular to the [111] fiber axis of the wires. This implies that a random area analysis of the precipitates along a [111] direction, via the pulsed field-evaporation technique, results in the uncovering of Cu/MgO (111) heterophase interfaces.

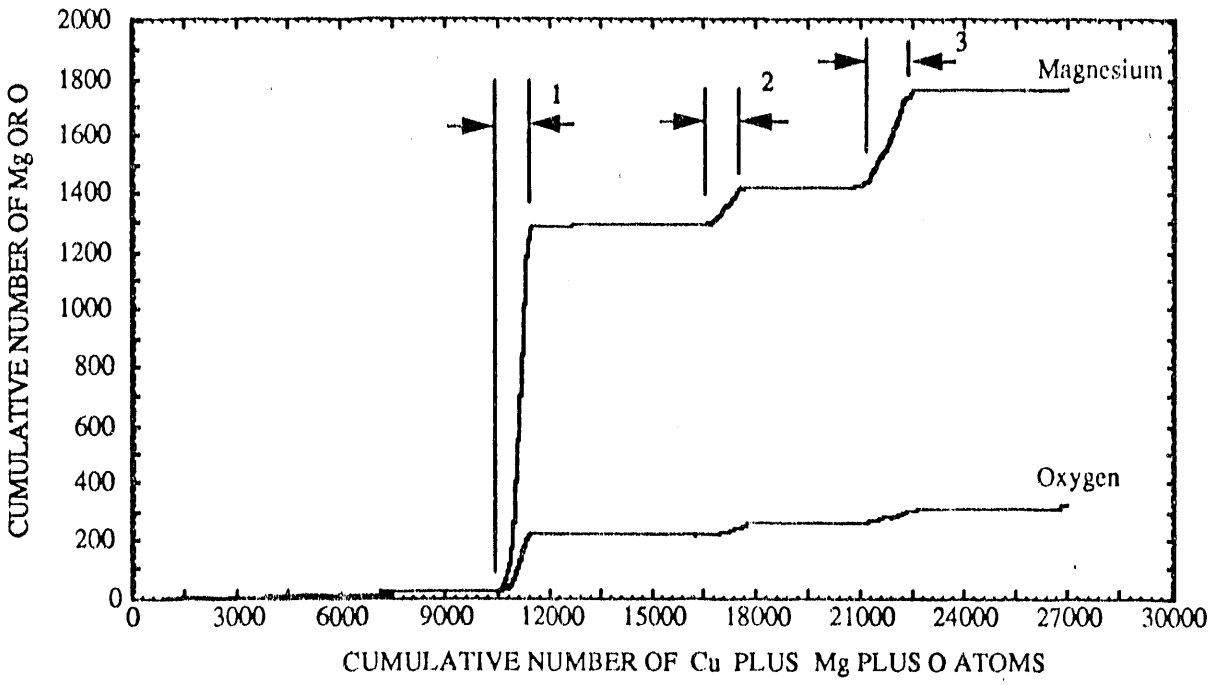

FIG. 16. Integral profiles for Mg and O accumulated during a random area analysis of a copper FIM tip containing MgO precipitates along a [110] direction; the cumulative number of Mg or O ions is plotted against the cumulative number of Cu plus Mg plus O ions. The data were collected for a specimen temperature of 35 K, a pulse fraction of 0.1, a pulse frequency of 15 Hz, and a background pressure of $1.2 \cdot 10^{-8}$ Pa. The regions numbered 1, 2 and 3 correspond to heterophase fluctuations.

6. The Cu matrix is found, via atom probe field-ion microscopy, to be almost 100 at.% Cu, with only trace amounts of oxygen ($<10^{-3}$ at. fr.) and magnesium ($<10^{-4}$ at. fr.) after an internal oxidation treatment. No evidence was found for impurity atoms at the Cu/MgO (111) heterophase interface.

7. Atom-probe field-ion microscopy analyses reveal that the sequence of atoms across a Cu/MgO (111) interface is Cu|O|Mg|... and *not* Cu|Mg|O|... . Thus the terminating (222) plane for a MgO precipitate in a Cu matrix is oxygen and not magnesium. This result is achieved *without* any deconvolution of the experimental data. The resolution of the composition profile perpendicular to the interface is equal to the interplanar spacing of the $(222)_{MgO}$ planes and this value is 0.121 nm.

8. For a specimen in which the mean precipitate diameter was 10 nm evidence is found for the existence of heterophase fluctuations or cluster of MgO, for which the stoichiometric ratio is different from unity. This result cannot be explained on the basis of preferential field evaporation of Mg as the number of Mg atoms per cluster is greater than the number of O atoms.

References

1. Metal-Ceramic Interfaces: Proceedings of an International Workshop, edited by M. Rühle, A. G. Evans, M. F. Ashby and J. P. Hirth (Pergamon, Oxford, 1990).
2. Proceedings of the International Symposium on Metal/Ceramic Interfaces, edited by W. Mader and M. Rühle, Irsee, Germany, to appear 1992.
3. Structure and Properties of Intergranular Boundaries, J. Phys.(Paris) **43**, Colloque C-6, supplément au No. 12 (1982).
4. Proceedings of the International Conference on the Structure and Properties of Internal Interfaces, J. Phys. (Paris) **46**, Colloque C4, Supplément au No. 4 (1985).

5. Proceedings of the Interface Science and Engineering '87 Conference J. Phys. (Paris) C5-9, Colloque C5, supplément au No. 10 (1988).
6. Proceedings of the International Congress: Intergranular and Interphase Boundaries in Materials, Coll. Phys (Paris) **51**, Colloque C1, Supplément au No. 1 (1990).
7. G. Petzow, T. Suga, G. Elssner and M. Turwitt, in Sintered Metal-Ceramic Composites, edited by G. S. Upadhyaya (Elsevier, Amsterdam, 1984), p. 3.
8. H. Gleiter, Nanostructured Mater. **1**, 1 (1992).
9. Electronic Packaging in Materials Science, edited by E. A. Geiss, K. N. Tu and E. I. Ruhlmann, Mat. Res. Soc.Symp. Proc. **209** (1985).
10. H. Schmalzried, Ber. Bunsenges. Phys. Chem. **87**, 551 (1983); G. L. Kellogg, Science **171**, 359 (1986).
11. A. J. Freeman and Chun Li, in Metal-Ceramic Interfaces: Proceedings of an International Workshop, edited by M. Rühle, A. G. Evans, M. F. Ashby and J. P. Hirth (Pergamon, Oxford, 1990), p. 8; Chun Li and A. J. Freeman, Phys. Rev. B **43**, 780 (1991).
12. P. Blöchl, G. P. Das, H. F. Fischmeister, and U. Schönberger, in Metal-Ceramic Interfaces: Proceedings of an International Workshop, edited by M. Rühle, A. G. Evans, M. F. Ashby and J. P. Hirth (Pergamon, Oxford, 1990), pp. 9-14.
13. J. R. Smith, H. Schlosser, and J. Ferrante, in Metal-Ceramic Interfaces: Proceedings of an International Workshop, edited by M. Rühle, A. G. Evans, M. F. Ashby and J. P. Hirth (Pergamon, Oxford, 1990), pp. 15-24.
14. M. W. Finnis, A. M. Stoneham, and P. W. Tasker, in Metal-Ceramic Interfaces: Proceedings of an International Workshop, edited by M. Rühle, A. G. Evans, M. F. Ashby and J. P. Hirth (Pergamon, Oxford, 1990), pp. 35-44.
15. R. Gronsky, Ultramicroscopy, **24**, 155 (1988).
16. M. Rühle, K. Burger, and W. Mader, Microsc. Spectrosc. Electron. **11**, 163 (1986); G. Necker and W.Mader, Phil. Mag. Letts. **58**, 205 (1988); W. Mader, Z. Metallkde. **80**, 139 (1989).
17. W. Mader and G. Necker, in Metal-Ceramic Interfaces: Proceedings of an International Workshop, edited by M. Rühle, A. G. Evans, M. F. Ashby and J. P. Hirth (Pergamon, Oxford, 1990), pp. 222-233.
18. C. S. Smith, Min. and Met. **11**, 213 (1930); *idem, ibid.* **13**, 481 (1932); *idem*, J. Inst. Metals **46**, 49 (1931).
19. K. W. Fröhlich, Z. Metallk. **28**, 368 (1936).
20. F. N. Rhines, Trans. AIME, **137**, 246 (1940).
21. F. N. Rhines, W. A. Johnson, and W. A. Anderson, Trans. AIME **147**, 205 (1942).
22. C. Wagner, Z. Elektrochem. **63**, 772 (1959).
23. G. Böhm and M. Kahlweit, Acta Metall. **12**, 641 (1964); M. Kahlweit, Prog. Chem. Solid State **2**, 134 (1965).
24. R. A. Rapp, Corrosion-Nat. Assoc. Corr. Eng. **21**, 382 (1965).
25. J. L. Meijering, in Advances in Materials Research, edited by H. Herman (J. Wiley & Sons, New York, 1971), Vol. 5, pp. 1-81.
26. M. Hansen and K. Anderko, Constitution of Binary Alloys, 2nd ed. (McGraw-Hill, New York, 1958), pp. 594-596; R. Hultgren, P. D. Desai, D. T. Hawkins, M. Gleiser, and K. K. Kelley, Selected Values of the Thermodynamic Properties of Binary Alloys (American Society for Metals, Metals Park, Ohio, 1973), pp. 750-755.
27. J. H. Swisher and E. O. Fuchs, Trans. Metall. Soc. AIME **245**, 1789 (1969).
28. B. W. Krakauer, J. G. Hu, S. M. Kuo, R. L. Mallick, A. Seki, D. N. Seidman, J. P. Baker, and R. J. Loyd, Rev. Sci. Instrum. **61**, 3390 (1990).
29. M. F. Ashby and L. M. Brown, Phil. Mag. **8**, 1083 (1963).
30. D. J. Pedder, E. D. Boyes, and G. C. Smith, Metal Science J. **12**, 437 (1976).
31. R. Hattenbauer and F. Haider, Scripta Metall. Mater. **25**, 1173 (1991).
32. U. Dahmen, Ultramicroscopy **30**, 102 (1989).
33. W. Kesternich, Mat. Res. Soc. Symp. Proc. **62**, 229 (1986).
34. K. L. Merkle, Ultramicroscopy **37**, 130 (1991); in Metal-Ceramic Interfaces: Proceedings of an International Workshop, edited by M. Rühle, A. G. Evans, M. F. Ashby and J. P. Hirth (Pergamon, Oxford, 1990), pp.242-249; K. L. Merkle, M. I. Buckett, and Y. Gao, in proceedings of the International Symposium on Metal/Ceramic Interfaces, edited by W. Mader and M. Rühle, Irsee, Germany, to appear 1992.

35. P. Lu and Cosandey, in proceedings of the International Symposium on Metal/Ceramic Interfaces, edited by W. Mader and M. Rühle, Irsee, Germany, to appear 1992.
36. C. S. Barrett and T. B. Massalski, Structure of Metals , 3rd ed. (McGraw-Hill, New York, 1966), pp. 568-569.
37. B. W. Krakauer and D. N. Seidman, submitted to Rev. Sci. Instrum. (1992); D. Chan, D. N. Seidman and K. L. Merkle, unpublished research.
38. T. M. Hall , A. Wagner and D. N. Seidman, J. Phys. E: Sci. Instrum. **10**, 884 (1977).
39. D. N. Seidman, J. Phys. F: Metal Phys. **3**, 393 (1973); A. S. Berger, D. N. Seidman and R. W. Balluffi, Acta Metall. **21**, 123 & 134 (1973); D. N. Seidman, in Radiation Damage in Metals, edited by N. L. Peterson and S. D. Harkness (American Society for Metals, Metals Park, Ohio, 1976), pp. 28-57; D. N. Seidman, Mater. Res. Soc. Symp. Proc. **138**, 315 (1989); D. N. Seidman, Mater. Res. Soc. Symp. Proc. **139**, 25 (1989).
40. S. S. Brenner, Surf. Sci. 70, 427 (1978); S. S. Brenner and M. K. Miller, J. Metals **35** (3), 54 (1983).
41. R. Wagner, Field-Ion Microscopy (Springer-Verlag, Berlin, 1982), Chapt. 4, pp. 80-99.
42. P. Haasen, Metall. Trans. A **16A**, 1173 (1985); P. Haasen and R. Wagner, Ann. Rev. Mater. Sci. **15**, 43 (1985).
43. T. Sakurai, A. Sakai and H. W. Pickering, Atom-Probe Field-Ion Microscopy and Its Applications (Academic Press, New York, 1989), Chapt. 6, pp. 202-235.
44. D. Blavette and P. Auger, Microsc. Microanal. Microstruct. **1**, 481 (1990).
45. R. Herschitz and D. N. Seidman, Acta Metall. **32**, 1141 & 1155 (1984).
46. S. M. Kuo, A. Seki, Y. Oh, and D. N. Seidman, Phys. Rev. Lett. **65**, 199 (1990); J. G. Hu and D. N. Seidman, Phys. Rev. Lett. **65**, 1615 (1990); D. N. Seidman, Mater. Sci. Eng. **A137**, 57 (1991).
47. J. G. Hu, Ph.D. thesis, Northwestern University (1991); J. G. Hu and D. N. Seidman, submitted for publication (1991).
48. B. W. Krakauer, Ph.D. thesis, Northwestern University (1992).
49. J. Ho, D. N. Seidman, and K. L. Merkle, Scripta Metall. Mater. **26** (1992).
50. C. Kittel, Introduction to Solid State Physics, 6th ed. (John Wiley & Sons, New York, 1986), p. 55.
51. T. T. Tsong, Atom-Probe Field Ion Microscopy (Cambridge Univ. Press, Cambridge, 1990), pp. 31-41
52. M. K. Miller and G. D. W. Smith, Atom Probe Microanalysis (Materials Research Society, Pittsburgh, Pennsylvania, 1989), pp. 14-20, A30-A31.
53. J. W. Christian, The Theory of Transformations in Metals and Alloys (Pergamon Press, Oxoford, 1975), Part I, Chapt. 10, pp. 424-432.

B. Chemical Composition on an Atomic Scale of Ni/Cr_2O_3 Interfaces (Mr. David Chan, Ph.D. candidate)

1. Abstract

The chemical composition profiles across Ni/Cr_2O_3 interfaces are being studied employing atom-probe field-ion microscopy, inconjunction with transmission electron and high resolution microscopies to study the structure of interfaces. This heterophase interface is produced by internally oxidizing an Ni-1 at.% Cr alloy to produce hcp Cr_2O_3 precipitates. Thus, in this system the heterophase interface is between an fcc matrix and an hcp precipitate. A significant fraction of the Cr_2O_3 precipitates are faceted such that $(111)_{Ni}\|(0001)_{oxide}$ or $(110)_{Ni}\|(11\text{-}20)_{oxide}$. For Ni/Cr_2O_3 interfaces selected area atom-probe field-ion microscopy is employed as the number density of Cr_2O_3 is not high enough to employ the random area analysis technique; the latter technique is successful for the Cu/MgO system, because the number density of MgO precipitates is $\approx 5 \cdot 10^{21}$ m^{-3} -- see Section I.A. We have succeeded to backpolish field-ion microscope specimens containing Cr_2O_3 precipitates and to place these precipitates at a distance of <100 nm from the tip, and then to successfully field evaporate specimens to place Cr_2O_3 precipitates in the field-of-view of field-ion microscope images. Atom-probe field-ion microscope mass spectra and integral profiles have been obtained from these specimens. Experiments are presently in progress to analyze the chemical sequence across Ni/Cr_2O_3 interfaces in detail, and to determine the structure of these intefaces via high resolution electron microscopy.

2. Introduction

The atom-probe field-ion microscope technique is a powerful method for determining interfacial composition and the chemistry of individual precipitates on an atomic scale. Previous studies include, for instance, determining the chemical compositions of radiation induced precipitates [1,2], the composition of precipitates in aged Al-Li-Zr alloys [3], the compositions of precipitates produced by internal nitridation of binary alloys [4,5], and the compositions of precipitates formed in an initially single-phase solid-solution [6]. Recently at Northwestern we have determined the chemical sequence across a {111}-type interface between Cu and MgO formed via internal oxidation [7]; this study employs the random area analysis technique [8] to examine this interface. The random area analysis technique involves analyzing, via the time-of-flight technique, all the atoms contained in a cylinder of alloy on an atom-by-atom basis -- see Fig. 10. The volume of material analyzed in a well annealed specimen is typically 10^{-21} m^3. Thus, in order to encounter a precipitate, with a reasonably high probability, a high number density ($>10^{21}$ m^{-3}) of small precipitates (20 nm diam) is required within the analyzed volume. If the number density is $<10^{21}$ m^{-3} a number of samples may have to be examined before a precipitate is detected. In this situation the examination of a metal/ceramic interfaces can be facilitated by using the so-called selected area analysis technique [8].

The selected area analysis technique requires locating a precipitate within the field-of-view of an FIM image, and aligning the probe hole to cover an area less than that covered by the precipitate. When the precipitate number density is low tens of nm of material may have to be removed by the pulsed field-evaporation technique before a precipitate is encountered. The dissection of a tip by the pulsed field-evaporation technique is time consuming, with a finite probability of a tip fracturing as the electric field is increased. Alternatively, precipitates can be located within the tip volume of an FIM specimen, by transmission electron microscopy, if they are located within ≈100 nm of the tip. This geometry is achieved by electropolishing a specimen in a small diameter loop employing short highly controlled voltage pulses [9,10]. We have previously used this method to study grain boundary segregation by placing grain boundaries within 50 nm of a tip [9,10].

In this research, a systematic method is demonstrated in which internally oxidized Ni-1 at.% Cr alloy specimens are backpolished in a highly controlled manner, such that individual Cr_2O_3 precipitates are consistently placed within <100 nm from a tip. Nickel is fcc with a lattice constant of 3.5339 Å, and Cr_2O_3 is hcp with the oxygen atoms on the hcp sites and the chromium atoms on the octahedral sites. For hcp Cr_2O_3 the lattice constant a is 4.954 Å, and the lattice constant c is 13.584 Å. The misfit parameter (η) is given by $\eta = 2[(a_{oxide} - a_{Ni})/(a_{oxide} + a_{Ni})]$. The value of η along the $\langle 111\rangle_{Ni} \| \langle 0001\rangle_{oxide}$ is 66%; this corresponds to the close-packed $\{111\}_{Ni}$ planes parallel to the close-packed $\{0001\}_{oxide}$ basal planes. Precipitates of Cr_2O_3 were obtained by internal oxidation of a Ni-1 at.% Cr alloy with a size range of 50 to 150 nm, and at a low number density ($<10^{-21}$ m^3). We have developed the selected area technique for examining the interfacial region between Ni and Cr_2O_3 precipitates, as the number density of Cr_2O_3 precipitates is too small to use the random area analysis technique as was done for Cu/MgO interfaces. We are able to place selectively a Cr_2O_3 precipitate with the volume of a tip, so that it can be analyzed chemically by the atom probe technique. The technique used employs electrolytic polishing using voltage pulses as short 80 μs to remove nm of material. Examples of the application of this technique are presented, along with atom probe data -- a mass spectrum and an integral profile -- for this system.

3. Experimental Procedures

A Ni(Cr) alloy is prepared from Ni (Materials Research Corporation, Marz grade, 99.995% pure) and Cr (Johnson Matthey, 99.99% pure) by arc melting these elements three times in an argon atmosphere. The

alloy is homogenized at 850°C for 100 hours, cold swaged to a 0.16 cm diam rod, and drawn into 134 μm diam wire. The as-drawn wire is electrolytically thinned to a sharply tapering tip (10 nm radius) in a 40% HCl solution. The thinned wires are annealed at 900°C for 30 minutes in an evacuated quartz tube (30 mTorr) containing a Rhines pack [11] consisting of a Ni:NiO (1:3) powder mixture. This Rhines pack mixture forms an oxygen atmosphere within the tube that is less than the partial pressure required for the formation of stable NiO, but is greater than the partial pressure required for the formation of stable Cr_2O_3.

The tips undergo some blunting -- up to 15 times the initial diameter -- during annealing. They are resharpened using a sophisticated backpolishing setup developed at Northwestern University [12]. The backpolishing unit consists of a specially fabricated power supply that is gated using an E & L Instruments pulse generator. An optical microscope with an x-y translation stage is used to manipulate the tip of the wire within a small diameter (3 mm) Pt loop that serves as a cathode. The cathode loop contains, in the form of a meniscus, an electrolytic solution of H_3PO_4:butoxyethanol:H_2O (4:4:3). The power supply is gated by a pulse generator to apply pulses as short as 10 μsec to a tip. An electropolished tip is observed in an Hitachi 700H 200 kV transmission electron microscope, employing a specially modified double-tilt stage to hold a one cm long wire sample [12]. The precipitates are observed in a specimen employing standard transmission electron microscope diffraction techniques. If a Cr_2O_3 precipitate is not within 100 nm of a tip, the wire is backpolished until this condition is achieved. Using this combination of transmission electron microscopy and highly controlled electropolishing wires can be resharpened, and a Cr_2O_3 precipitate placed in the tip of an FIM specimen.

4. Results

An oxidized Ni-1 at.% Cr tip is shown in Fig. 17(a) after resharpening. Cr_2O_3 precipitates are clearly visible along the central axis of the wire. The tip is sharp (50 nm radius) with a shank angle of 30°. An 80 μs pulse is applied to the tip, and approximately 8 nm of material is removed from the tip along the axis of the wire -- Fig. 17(b). After further backpolishing, a precipitate is seen located at a distance of 176.8 nm from the tip -- Fig. 18(a). As the tip surface is not smooth, the tip is further backpolished with an 800 μs pulse -- Fig. 18(b). Approximately 80 nm of material is removed, and a smoother surface is obtained. The Cr_2O_3 precipitates are now within 100 nm from the tip, and this specimen is suitable for atom-probe analysis. Figure 19 is an example of another specimen prepared in the same manner. A Cr_2O_3 precipitate is clearly seen within 41.3 nm of the tip. Employing selected area diffraction we find that the facets parallel to the long faces have $(111)_{Ni} \parallel (0001)_{oxide}$ [that is, a close-packed plane in the Ni matrix parallel to a close-packed plane in the hcp Cr_2O_3 precipitate], and the facets parallel to the short faces have $(110)_{Ni} \parallel (11\bar{2}0)_{oxide}$. Thus, internally oxidized Ni-1 at.% Cr wire alloys -- containing Cr_2O_3 precipitates -- can be reproducibly sharpened, and specimens routinely backpolished to place Cr_2O_3 precipitates within 100 nm of a tip's surface.

Figure 20 shows the mass spectrum for an internally oxidized Ni-1 at.% Cr alloy. The dominant peak is due to Ni^{2+} since the matrix contains very little Cr or O after the internal oxidation treatment. Figure 21 is an integral profile, along a <112>-type direction, through an atom probe specimen that had been internally oxidized; the specimen temperature was 55 K and the pulse fraction -- ratio of the pulse voltage to the steady state dc voltage -- is 0.1. Note that a cluster consisting of seven oxygen and six chromium atoms is present in this profile, and that the matrix is pure Ni both before and after the cluster is detected. The total number of atoms detected is only 13 in this cluster, hence it is most likely a heterophase fluctuation.

5. Conclusions

A methodology for systematically producing internally oxidized Ni-1 at. % Cr alloys specimens suitable for combined transmission electron and atom-probe field-ion microscopies is presented. The technique developed allows us to selectively place Cr_2O_3 precipitates to within 100 nm of a tip's surface using a highly controlled electropolishing technique. The tip is then developed in the field-ion microscope by controlled dissection of a specimen, employing pulsed field-evaporation, until the selected precipitate is observed in a field-ion image, and then the probe hole is aligned over the precipitate. This procedure allows a selected area analysis of a precipitate to be performed through the interfacial region between the matrix and the precipitate. Examples are given of this approach for two different specimens, and an integral profile exhibiting a heterophase fluctuation of O and Cr is exhibited. Experiments are currently in progress to obtain the interfacial chemical sequence across known crystallographic planes between the Ni matrix and a Cr_2O_3 precipitate as was done for the Cu/MgO {111} interface [7]. Experiments are presently in progress to analyze the chemical sequence across Ni/Cr_2O_3 interfaces in detail, and to determine the structure of these intefaces via high resolution electron microscopy.

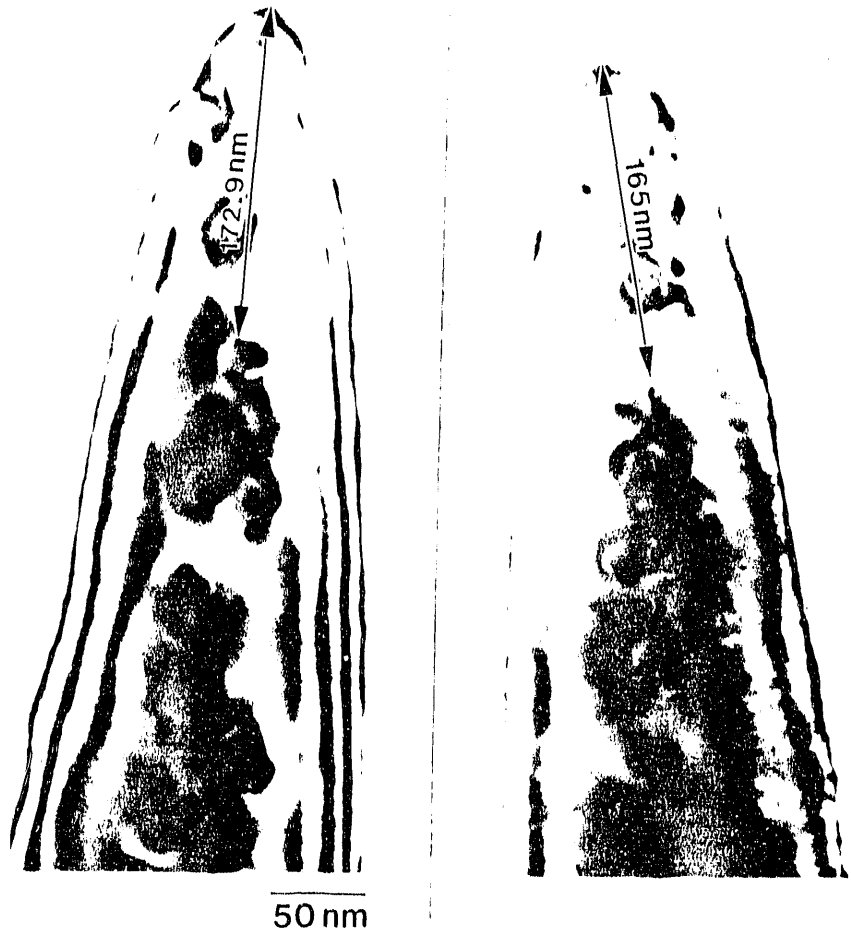

FIG. 17 (a) A Ni-1 at.% Cr that had been resharpened electrolytically after internal oxidation at 900°C for 30 min. (b) Same wire specimen after electrolytic backpolishing with an 80 μs pulse.

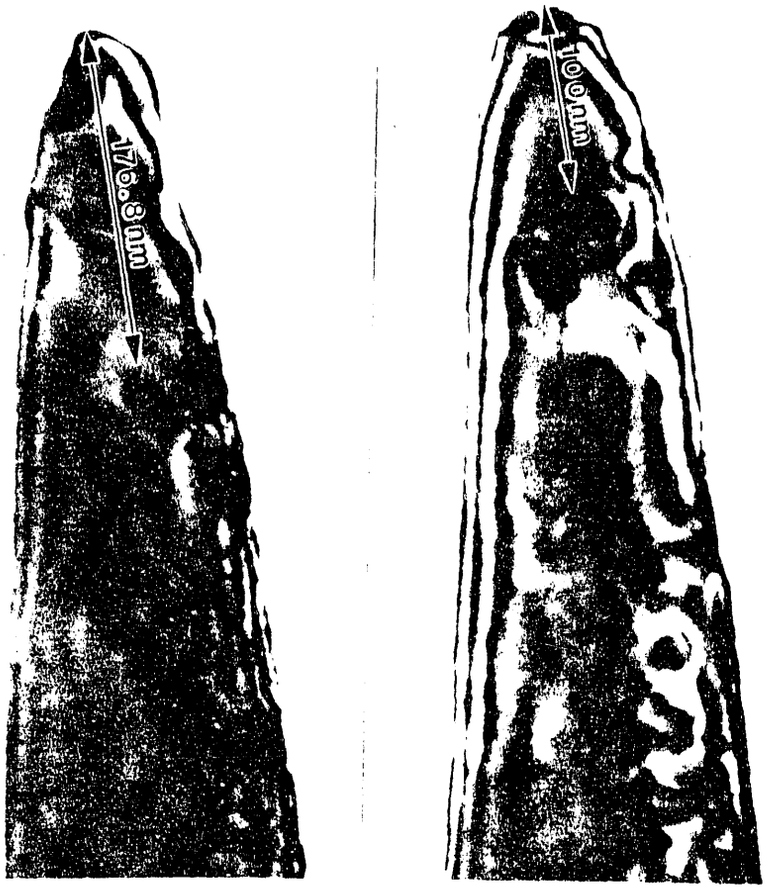

FIG. 18 (a) Same wire specimen as in Fig. 17 after futher backpolishing. (b) After an additional electrolytic backpolishing with an 800 μs voltage pulse.

Fig. 19 Another Ni-1 at.% Cr specimen internally oxidized at 900°C for 30 min and electrolytically backpolished to a sharp tip. Note the presence of a highly faceted Cr_2O_3 precipitate 41.3 nm from the tip.

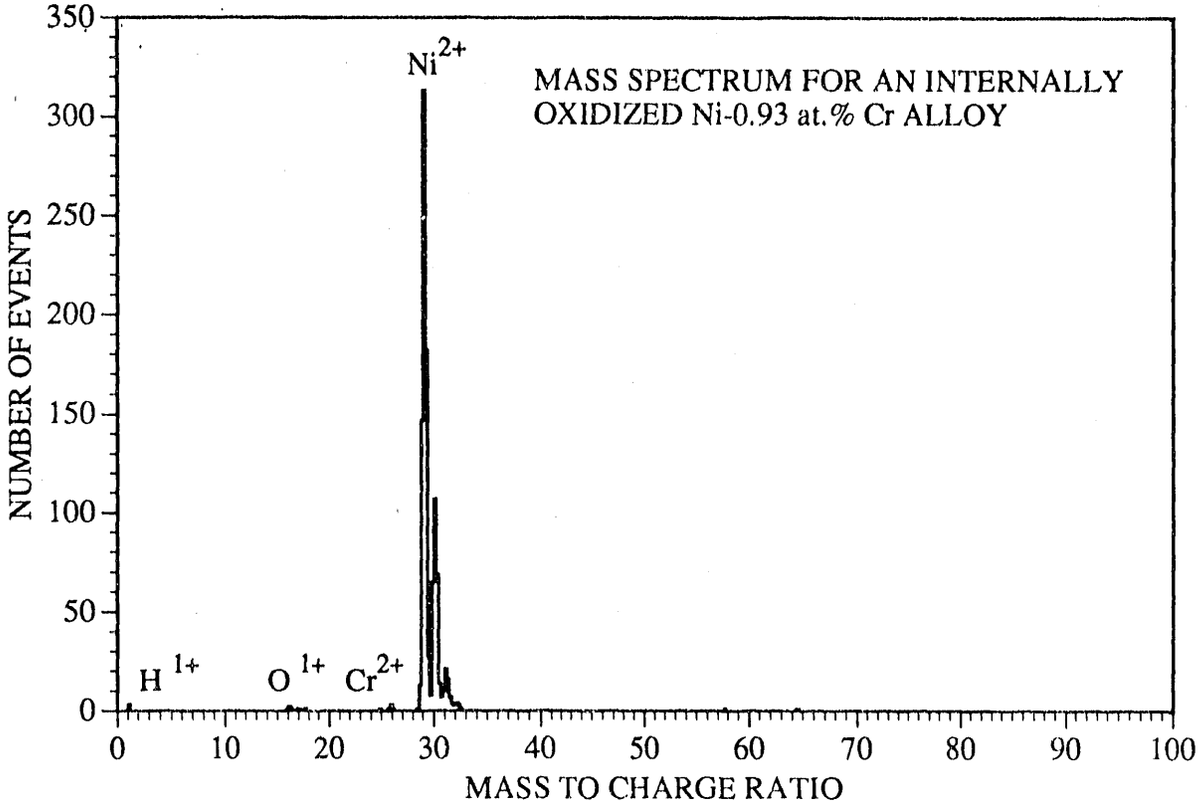

FIG. 20 A mass spectrum of the number of events versus the mass-to-charge state ratio of a Ni-1 at.% Cr alloy that had been internally oxidized at 900°C for 30 min.

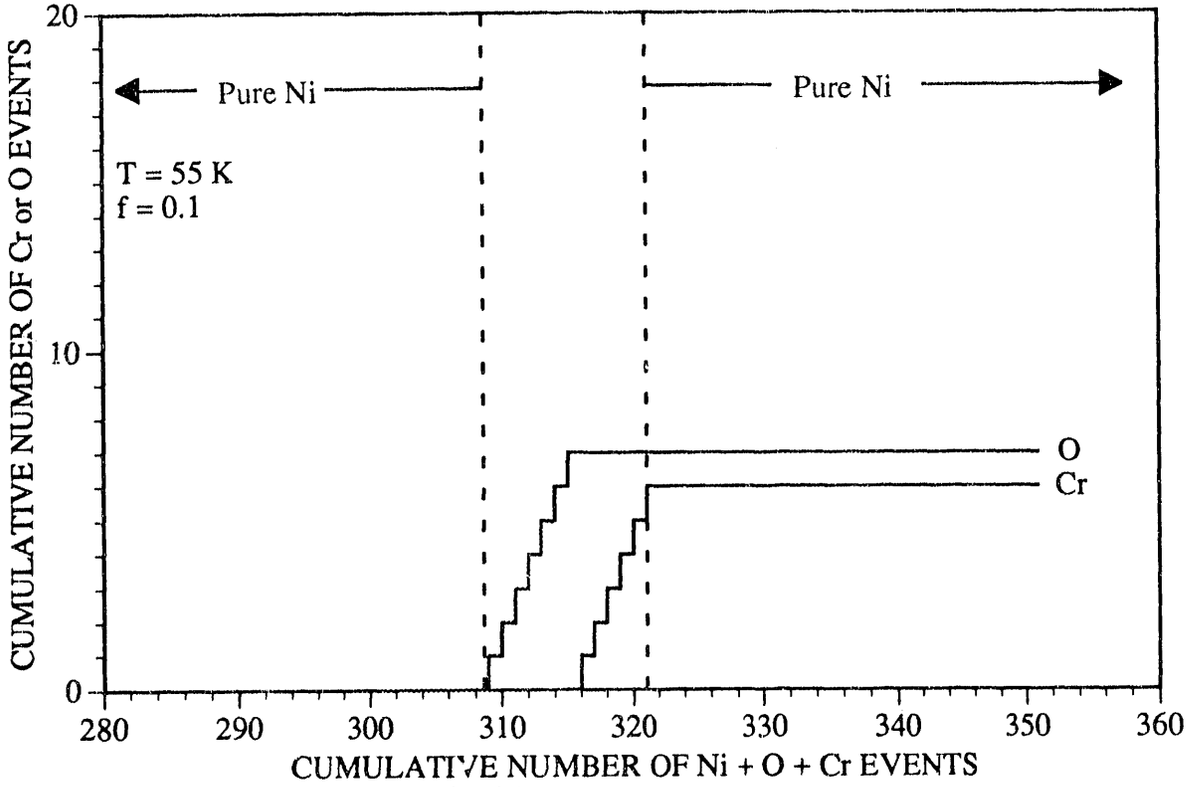

FIG. 21 An integral profile through the same specimen, along a <112>-type direction in the Ni matrix, for which a mass spectrum is displayed in Fig. 20. This integral profile contains a cluster of 13 O and Cr atoms. Note that both before and after the cluster that the matrix is pure Ni.

References

1. R.Herschitz and D. N. Seidman, Acta Metall. **32**, 1141 (1984).
2. R.Herschitz and D. N. Seidman, Acta Metall. **32**, 1155 (1984).
3. T. Abe, Scripta Metall. Mater. **26**, 1143 (1992).
4. R. Wagner and S. S. Brenner, Acta Metall. **26**, 197 (1978).
5. S. Chambreland, A. Walder, and D. Blavette, Acta Metall. **36**, 3205 (1988).
6. K. Hono, H. W. Pickering, and T. Sakurai, Scripta Metall. **22**, 881 (1988).
7. H. Jang, D. N. Seidman, and K. L. Merkle, Scripta Metall. Mater. **26**, 1493 (1992).
8. M. K. Miller, Int. Mat. Rev. **32**, 221 (1987).
9. J. G. Hu and D. N. Seidman, Phys. Rev. Lett. **65**, 1615 (1990); J. G. Hu, Ph.D. Thesis, Northwestern University 1991; J. G. Hu and D. N. Seidman, submitted to Philos. Mag. Lett. (1992).
10. B. W. Krakauer and D. N. Seidman, submitted to Rev. Sci. Instrum. (1992).
11. F. N. Rhines, Trans AIME **137**, 246 (1940).
12. B. W. Krakauer, J. G. Hu, S.-M. Kuo, R. L. Mallick, A. Seki, D. N. Seidman, J. P. Baker, and R. J. Loyd, Rev. Sci. Instrum. **61**, 3390 (1990).

END

DATE
FILMED
6/09/92